Organometallics 1991, *10*, 3861–3873

Oxidative Transformation of $[^{R}Cp(CO)_2MnSR]^\bullet$ Radicals into "Inidene" Compounds $[^{R}Cp(CO)_2Mn]_2SR^+$

Patrizia Lau, Horst Braunwarth, Gottfried Huttner,* Diethelm Günauer, Kaspar Evertz, Wolfgang Imhof, Christiane Emmerich, and Laszlo Zsolnai

Anorganisch-Chemisches Institut der Universität Heidelberg, Im Neuenheimer Feld 270, D-6900 Heidelberg, Germany

Received June 24, 1991

Stable radical compounds $[^{R}Cp(CO)_2MnSR]^\bullet$ (^{R}Cp = Cp, Cp′, Cp*; $1^\bullet$) have been obtained by air oxidation of the primary products formed from RSH and $^{R}Cp(CO)_2Mn(THF)$ for a wide variety of alkyl and aryl substituents R. EPR spectra and bulk susceptibility measurements together with solution and solid-state UV/vis spectra show that compounds $1^\bullet$ are stable monomeric radicals. Preparative oxidation of $1^\bullet$ by $AgPF_6$ yields the binuclear species $[^{R}Cp(CO)_2Mn]_2SR^+PF_6^-$ ($[2^+][PF_6^-]$). The cations 2^+ exist either as "inidene"-type compounds $L_nM\underset{\cdots}{-}S(R)\underset{\cdots}{-}ML_n$ (L_nM = $^{R}Cp(CO)_2Mn$) with a trigonal-planar coordination at the bridging sulfur or in the ring-closed isomeric form $[L_n\overline{M\text{—}S(R)\text{—}M}L_n]^+$ with a metal–metal bond and a pyramidal sulfur. The two isomeric forms of 2^+ are easily distinguished by their UV/vis spectra. Intense long-wavelength π–π^* absorptions are characteristic of the inidene-type isomers. Cyclic voltammetry reveals reversible one-electron redox reactions for $1^\bullet$ as well as for $2^\bullet$ corresponding to $1^- \rightleftharpoons 1^\bullet \rightleftharpoons 1^+$ and $2^- \rightleftharpoons 2^\bullet \rightleftharpoons 2^+$, respectively. It is observed that the reduction of 1^+ is about 500 mV less negative as compared to the reduction of 2^+ throughout. This finding corresponds to the relative stability of the LUMO's of 1^+ (olefinic type π-system) versus those of 2^+ (allylic type π-system) as visualized by qualitative MO reasoning. X-ray structural data are presented for $[^{R}Cp(CO)_2MnSR]^\bullet$ (^{R}Cp = Cp, R = Ph, $1a^\bullet$; ^{R}Cp = Cp′, R = C_6F_5, $1f^\bullet$) and $[^{R}Cp(CO)_2Mn]_2SR^+PF_6^-$ (^{R}Cp = Cp, R = $^{p}NO_2$-C_6H_4, $[2b^+][PF_6^-]$; ^{R}Cp = Cp′, R = ^{i}Pr, $[2h^+][PF_6^-]$; ^{R}Cp = Cp′, R = ^{t}Bu, $[2i^+][PF_6^-]$).

Introduction

With the general aim of extending the chemistry of "inidene" compounds $[L_nM\underset{\cdots}{-}E(R)\underset{\cdots}{-}ML_n]^m$ [1] (L_nM = 16-electron organometallic fragment, ER^m = six-electron main-group species) to group 16 bridging entities RS^+, syntheses and properties of the species $[^{R}Cp(CO)_2MnSR]^\bullet$ ($1^\bullet$; ^{R}Cp = Cp, Cp′, Cp*) have been studied, which upon preparative oxidation yield the binuclear compounds $[^{R}Cp(CO)_2Mn]_2SR^+$ (2^+).

Compounds $1^\bullet$ are notable substances in themselves, since they represent rare examples of mononuclear organometallic radical species. The only two examples of type $1^\bullet$ radicals previously described are $[Cp^*(CO)_2MnSR]^\bullet$ (R = ^{t}Bu ($1m^\bullet$), adamantyl);[2,3] it might be argued that these molecules are stable as monomeric radicals because of the steric shielding imposed by the bulky Cp* and R residues. The series of compounds $1^\bullet$ with less bulky substituents (least demanding set ^{R}Cp = Cp, R = Et ($1j^\bullet$)) has been synthesized in order to substantiate the hypothesis that the propensity of compounds $1^\bullet$ to exist as monomeric radicals, not undergoing dimerization, is an inherent property of $1^\bullet$.

In this case compound $1^\bullet$ should be monomeric, independent of the steric conditions. The difference between the stable radical complexes $1^\bullet$ and their elusive isoelectronic analogues $[(CO)_5CrSR]$,[4] which have a half-life of only around 50 μs, must then be intimately connected to the difference in the fine tuning of the electronic properties of the two 16-electron L_nM species $^{R}Cp(CO)_2Mn$ and $(CO)_5Cr$, respectively.

The analogous nature of all the members of the series of compounds $1^\bullet$, independent of the individual steric conditions, should further be evident from their redox behavior: for $[Cp^*(CO)_2MnSR]^\bullet$ (R = ^{t}Bu ($1m^\bullet$), adamantyl)[2,3] reversible one-electron-reduction as well as -oxidation waves had been observed[3] which should then similarly be found for the other members of the family of compounds $1^\bullet$.

Preparative oxidation of $[Cp(CO)_2MnSPh]^\bullet$ ($1a^\bullet$), with $AgPF_6$ as an oxidant, had led to the binuclear inidene-type compound $[Cp(CO)_2Mn]_2SPh^+$ ($2a^+$),[5] the properties of which correspond in every comparable detail to the properties of the well-characterized isoelectronic phosphinidene complexes $L_nM\underset{\cdots}{-}P(R)\underset{\cdots}{-}ML_n$.[1] On the other hand, Haines et al. had shown that $[Cp'(CO)_2Mn]_2SEt^+$ ($2g^+$)[6] obtained by a different synthetic approach exists in the isomeric form with a closed metal–metal-bonded triangle $\overline{Mn\text{—}S(R)\text{—}Mn}$ and a pyramidally coordinated sulfur center.[6]

The question of valence isomerism conceivable for inidene compounds has been addressed experimentally by different groups[7-10] with stibinidene species $[(CO)_5W]_2SbR$, which without exception exist in the open form with no metal–metal bond and trigonal-planar-coordinated antimony; trapping experiments with Lewis acids indicate a valence-isomeric equilibrium between the open inidene-type geometry and the ring-closed isomer.[7] In the case of $[(CO)_4Fe]_2SbR$ the Fe–Fe-bonded isomer has been characterized as the stable isomer in the solid state.[9] Finally, an equilibrium between the inidene-type structure and the corresponding ring-closed isomeric geometry has been

---

[1] For a review, see: (a) Huttner, G.; Evertz, K. *Acc. Chem. Res.* **1986**, *19*, 406. (b) Huttner, G. *Pure Appl. Chem.* **1986**, *58*, 585.

[2] Winter, A.; Huttner, G.; Zsolnai, L.; Kroneck, P.; Gottlieb, M. *Angew. Chem.* **1984**, *96*, 986; *Angew. Chem., Int. Ed. Engl.* **1984**, *23*, 975.

[3] Winter, A.; Huttner, G.; Gottlieb, M.; Jibril, I. *J. Organomet. Chem.* **1985**, *286*, 317.

[4] Springs, J.; Janzen, C. P.; Darensbourg, M. Y.; Calabrese, J. C.; Krusic, P. J.; Verpeaux, J.-N.; Amatore, C. *J. Am. Chem. Soc.* **1990**, *112*, 5789.

[5] Braunwarth, H.; Huttner, G.; Zsolnai, L. *Angew. Chem.* **1988**, *100*, 731; *Angew. Chem., Int. Ed. Engl.* **1988**, *27*, 698.

[6] Burckett-St. Laurent, J. C. T. R.; Caira, M. C.; English, R. B.; Haines, R. J.; Nassimbeni, L. R. *J. Chem. Soc., Dalton Trans.* **1977**, 1077.

[7] Weber, U.; Huttner, G.; Scheidsteger, O.; Zsolnai, L. *J. Organomet. Chem.* **1985**, *289*, 357.

[8] Arif, A. M.; Cowley, A. H.; Norman, N. C.; Orpen, A. G.; Pakulski, M. *J. Chem. Soc., Chem. Commun.* **1985**, 1267.

[9] (a) Cowley, A. H. Norman, N. C.; Pakulski, M. *J. Am. Chem. Soc.* **1984**, *106*, 6844. (b) Cowley, A. H.; Norman, N. C.; Pakulski, M.; Bricker, D. L.; Russell, D. H. *J. Am. Chem. Soc.* **1985**, *107*, 8211.

[10] (a) Braunwarth, H.; Ettel, F.; Huttner, G. *J. Organomet. Chem.* **1988**, *355*, 281. (b) Lau, P.; Huttner, G. Zsolnai, L. *Z. Naturforsch.* **1991**, *46B*, 719.

0276-7333/91/2310-3861$02.50/0

directly observed for $[\mathrm{Cp(CO)_2Mn}]_2\mathrm{SePh}^+$,[10] the heavier isoelectronic analogue of $[{}^{\mathrm{R}}\mathrm{Cp(CO)_2Mn}]_2\mathrm{SR}^+$ (**2**$^+$). Considering these results, it appeared attractive to study the preparation of $[{}^{\mathrm{R}}\mathrm{Cp(CO)_2Mn}]_2\mathrm{SR}^+$ (**2**$^+$) from the mononuclear precursors **1**$^\bullet$. It was hoped that by the appropriate variation of R some further examples of inidene-type compounds $[\mathrm{Mn}\overset{\cdots}{-}\mathrm{S(R)}\overset{\cdots}{-}\mathrm{Mn}]^+$ might be obtained.

Herein we report the syntheses and properties of the mononuclear radical complexes $[{}^{\mathrm{R}}\mathrm{Cp(CO)_2MnSR}]^\bullet$ (**1**$^\bullet$) for a wide variety of substituents R.

EPR data and magnetic susceptibility measurements as well as X-ray structure analyses show that all the compounds are stable as monomeric entities. Cyclic voltammetry ranks compounds **1**$^\bullet$ into one class. One-electron reduction and one-electron oxidation are generally both reversible. Preparative oxidation of **1**$^\bullet$ leads to the corresponding dinuclear cations $[{}^{\mathrm{R}}\mathrm{Cp(CO)_2Mn}]_2\mathrm{SR}^+$ (**2**$^+$) in each case. X-ray analyses and spectra show that within the series of compounds **2**$^+$ the ones with R = alkyl exist as the ring-closed isomers while those with R = aryl, independent of the type of substitution at the aryl residue, are stable as the ring-opened inidene-type species. Cyclic voltammetry demonstrates that complexes **2**$^+$ undergo two reversible one-electron reductions corresponding to the occupation of the π^* LUMO within the three-center–four-π-electron systems of the inidene-type compounds **2**$^+$[5] by one and two electrons, respectively. The redox behavior of $\mathbf{2}^+ \rightleftharpoons \mathbf{2}^\bullet \rightleftharpoons \mathbf{2}^-$ is thus very much similar to the reversible one-electron oxidation of $[\mathrm{(CO)_5Cr}]_2\mathrm{SR}^-$.[4] While the dinuclear radicals **2**$^\bullet$ have not been isolated, the anion $[\mathrm{Cp'(CO)_2Mn}]_2\mathrm{SMes}^-$ (**2e**$^-$)[11] has been fortuitously obtained as a byproduct in another type of reaction. X-ray analysis and cyclic voltammetry of **2e**$^-$ are helpful in assessing the cyclic voltammetric behavior of the compounds **2**$^+$.

Experimental Section

All preparations and reactions were carried out with exclusion of air and moisture, by use of Schlenk techniques. Nitrogen was purified with use of BASF BTS catalyst for removal of oxygen and molecular sieves (3 Å, Merck) for absorption of water. The solvents tetrahydrofuran (THF), toluene, and $\mathrm{Et_2O}$ were freshly distilled over sodium; methylene chloride and *n*-pentane were distilled over calcium hydride. The stationary phases for column chromatography were deaerated at 10^{-2} mbar (20 °C; silica gel, J. T. Baker, 0.05—0.2 mm; silanized silica gel 60, Merck, 0.063–0.2 mm).

The thiols RSH and disulfides RSSR were purchased (Fluka) if not stated otherwise; $\mathrm{Cp'Mn(CO)_3}$ was from Janssen Chemicals. $\mathrm{CpMn(CO)_3}$ was obtained as a gift from Prof. Dr. D. Sellmann, Erlangen, Germany.

Photochemistry was performed with a mercury high-pressure bulb (TQ 150, Hanau; Pyrex) at a reaction temperature of 10 °C.

Melting points were determined with a Gallenkamp MFB-595 melting point apparatus and are uncorrected.

Elemental analyses were performed in the microanalytical laboratories of the Universities of Heidelberg and Konstanz.

IR spectra were measured in 0.1-mm $\mathrm{CaF_2}$ solution cells on a Perkin-Elmer 983-G spectrometer.

UV/vis spectra were obtained on a Perkin-Elmer Lambda 9 spectrometer; low-temperature measurements were performed on the same instrument with use of an Oxford Instruments liquid-nitrogen-cooled cryo compartment (Dn-1704) and temperature controller (ITC-4). For reflectance spectra the spectrometer was fitted with a diffuse-reflectance sphere (Perkin-Elmer).

EPR spectra were recorded with a Varian E3 spectrometer using quartz probe tubes; calibration was done with LiTCNQ (g = 2.0025).

^{1}H NMR spectra were taken on a Bruker AC 200 (200 MHz) spectrometer (internal standard acetone-d_6 (δ = 2.04 ppm), $\mathrm{CD_2Cl_2}$ (δ = 5.32 ppm) relative to external TMS). ^{19}F NMR data were obtained with a JEOL FX 90 Q (84 MHz) instrument (external standard $\mathrm{CFCl_3}$ (δ = 0 ppm)).

Bulk susceptibility measurements were made on a Faraday balance constructed from a Bruker BC-8 magnet (working field 6.12 kG) and a Sartorius 3044 balance. Calibration of the experimental setup was done by using $\mathrm{Co[Hg(SCN)_4]}$ ($10^6\chi_g$ = 16.45 emu/g at 293 K) as the standard.

Mass spectra were measured on a Finnigan MAT 8200 instrument. Positive ion spectra for neutral compounds (**1**$^\bullet$) were obtained by EI techniques (70 eV). For salt type compounds $[\mathbf{2}^+][\mathrm{PF_6}^-]$, the DCI technique was applied with isobutane as the reactant gas; the source temperature during these measurements was kept at 200 °C.

Cyclic voltammograms were measured with a Princeton Applied Research 273 potentiostat equipped with a BBC/Servogor (XY 733) plotter as the recording instrument. Electrochemistry was done in a gastight thermostated "Universal Meß- und Titriergefäß" equipment (Metrohm). A platinum wire (diameter 0.3 mm) was used as the counter electrode; the reference electrode consisted of a Radiometer K 401 saturated calomel electrode. The working electrode consisted of a circular glassy-carbon electrode (diameter 3 mm) fitted to a Metrohm RDE 628 building block. The supporting electrolyte was either $\mathrm{CH_2Cl_2}$ or $\mathrm{CH_3CN}$ with 0.1 M $\mathrm{Bu_4NPF_6}$. The concentration of the electroactive organometallic species was generally 0.001 M. The voltammograms were registered with a scan rate of 200 mV/s.

$[{}^{\mathrm{R}}\mathrm{Cp(CO)_2MnSR}]^\bullet$ (1$^\bullet$). A. In a typical preparation, 2 g of $^{\mathrm{R}}\mathrm{CpMn(CO)_3}$ ($^{\mathrm{R}}$Cp = Cp, 9.8 mmol; $^{\mathrm{R}}$Cp = Cp′, 9.2 mmol) was dissolved in THF (200 mL) and the solution irradiated for 3–4 h at 10 °C. To the resulting dark red solution of $^{\mathrm{R}}\mathrm{Cp(CO)_2Mn(THF)}$[12] (70%) was added 1 equiv of the corresponding thiol (see Table I) and the mixture stirred for 8 h at room temperature. A yellow-orange solution was obtained, though which air was passed for 1 min. This caused an instantaneous color change to either bright red or dark blue (see Table V). The resulting solution was absorbed on silica gel (5 g), and purification by column chromatography (silica gel, 50 cm × 3 cm, −25 °C) afforded three fractions: an initial yellow fraction (*n*-pentane), $^{\mathrm{R}}\mathrm{CpMn(CO)_3}$, a second green fraction (*n*-pentane–$\mathrm{CH_2Cl_2}$, 10:1), $[{}^{\mathrm{R}}\mathrm{Cp(CO)_2Mn}]_2\mathrm{S}$,[13] and a third red or blue fraction (for solvent mixture see Table I), $[{}^{\mathrm{R}}\mathrm{Cp(CO)_2MnSR}]^\bullet$ (**1**$^\bullet$). Crystallization from *n*-pentane–$\mathrm{CH_2Cl_2}$ (5:1) mixtures at −30 °C afforded the compounds **1**$^\bullet$ as crystalline products (yields are given in Table I).

B. When RSSR is used in place of RSH (e.g. compound **1b**$^\bullet$), the preparation is analogous to that described above (A) except that no oxidation is necessary.

The mass spectroscopic data for the series of compounds **1**$^\bullet$ are given in Table II.

$[{}^{\mathrm{R}}\mathrm{Cp(CO)_2Mn}]_2\mathrm{SR^+PF_6^-}$ ($[\mathbf{2}^+][\mathrm{PF_6}^-]$). To a stirred solution of **1**$^\bullet$ (amounts given in Table III) in toluene (20 mL) was added 1 equiv of $\mathrm{AgPF_6}$. The resultant mixture was stirred for a further 20 min at room temperature, during which time a dark precipitate was formed. The solvent volume was reduced to 5 mL in vacuo, and pentane (10 mL) was added; this further precipitated the crude product and also extracted $^{\mathrm{R}}\mathrm{CpMn(CO)_3}$ formed as a byproduct in the reaction. The suspension was then filtered through silanized silica gel 60 (5 cm) to remove any residual $^{\mathrm{R}}\mathrm{CpMn(CO)_3}$. Subsequent elution with $\mathrm{CH_2Cl_2}$ afforded $[\mathbf{2}^+][\mathrm{PF_6}^-]$.

The complexes were crystallized from $\mathrm{CH_2Cl_2}$–$\mathrm{Et_2O}$ (1:1) mixtures at −30 °C. A second recrystallization afforded analytically pure samples, and in the case of $[\mathbf{2a}^+][\mathrm{PF_6}^-]$,[5] $[\mathbf{2b}^+][\mathrm{PF_6}^-]$, $[\mathbf{2h}^+][\mathrm{PF_6}^-]$, and $[\mathbf{2i}^+][\mathrm{PF_6}^-]$ the crystals were suitable for X-ray diffraction studies.

An alternative preparation was used for the synthesis of the compounds $[\mathrm{Cp'(CO)_2Mn}]_2\mathrm{SEt^+PF_6^-}$ ($[\mathbf{2g}^+][\mathrm{PF_6}^-]$) and $[\mathrm{Cp'(CO)_2Mn}]_2\mathrm{S^tBu^+PF_6^-}$ ($[\mathbf{2i}^+][\mathrm{PF_6}^-]$): to the yellow-orange solution obtained from the reaction of $^{\mathrm{R}}\mathrm{Cp(CO)_2Mn(THF)}$ and RSH (see

---

[11] Ettel, F.; Huttner, G.; Zsolnai, L. *J. Organomet. Chem.*, in press.

[12] (a) Fischer, E. O.; Herberhold, M. *Essays in Coordination Chemistry*; Birkhäuser Verlag: Basel, Switzerland, 1964; Exper. Suppl. 9, p 259. (b) Strohmeier, M. *Angew. Chem.* **1964**, *76*, 873; *Angew. Chem., Int. Ed. Engl.* **1964**, *3*, 749.

[13] (a) Schneider, R. J. J. Dissertation, Technische Universität München, 1968. (b) Höfler, M.; Baitz, A. *Chem. Ber.* **1976**, *109*, 3147.

[14] Wang, C. H.; Cohen, S. G. *J. Am. Chem. Soc.* **1957**, *79*, 1924.

Table I. Analytical Data for the Compounds [^{R}Cp(CO)$_2$MnSR]• (1•)

compd	thiol; amt, g (mmol)	solvent mixture, ratio	yield,[c] mg (%)	mp,[d] °C	formula (M_r)	anal. % found (% calcd)
1a•	PhSH; 0.8 (7.0)	pentane–Et$_2$O, 4:1	620 (31)	100	$C_{13}H_{10}MnO_2S$ (285.22)	C, 54.67 (54.74) H, 3.62 (3.53) Mn, 19.05 (19.26)
1b•[a]	[^{p}NO$_2$C$_6$H$_4$S]$_2$; 1.1 (4.0)	pentane–CH$_2$Cl$_2$, 3:2	890 (34)			
1c•	^{p}TolSH; 0.8 (6.4)	pentane–CH$_2$Cl$_2$, 3:1	870 (43)	99	$C_{15}H_{14}MnO_2S$ (313.28)	C, 57.28 (57.51) H, 4.55 (4.50) S, 10.10 (10.24)
1d•	^{p}AnSH; 0.8 (6.5)	pentane–CH$_2$Cl$_2$, 2:1	820 (38)	46	$C_{15}H_{14}MnO_3S$ (329.28)	C, 54.69 (54.72) H, 4.37 (4.29)
1e•	MesSH;[b] 1.0 (6.6)	pentane–CH$_2$Cl$_2$, 3:1	940 (42)	66	$C_{17}H_{18}MnO_2S$ (341.33)	C, 59.70 (59.82) H, 5.50 (5.32) S, 9.48 (9.39)
1f•	C$_6$F$_5$SH; 1.3 (6.5)	pentane–CH$_2$Cl$_2$, 4:1	1110 (43)	100	$C_{14}H_7F_5MnO_2S$ (389.20)	C, 43.37 (43.21) H, 1.92 (1.81) S, 7.95 (8.24)
1j•	EtSH; 0.4 (7.0)	pentane–Et$_2$O, 4:1	930 (56)		$C_9H_{10}MnO_2S$ (237.18)	C, 45.72 (45.58) H, 3.56 (4.25) Mn, 23.00 (23.16)
1k•	^{i}PrSH; 0.5 (7.0)	pentane–Et$_2$O, 3:1	740 (41)		$C_{10}H_{12}MnO_2S$ (251.21)	C, 45.96 (47.81) H, 3.61 (4.81) Mn, 24.76 (21.87)
1l•	^{t}BuSH; 0.6 (7.0)	pentane–toluene, 7:3	930 (50)	75	$C_{11}H_{14}MnO_2S$ (265.23)	C, 49.08 (49.81) H, 5.49 (5.32)

[a] See preparation B. [b] See ref 14. [c] Yields based on sulfur. [d] Decomposition.

Table II. Mass Spectra of the Compounds [^{R}Cp(CO)$_2$MnSR]• (1•)

	MS, m/z (rel intens, %)							
fragment ion	**1a**•, R = Ph, ^{R}Cp = Cp	**1c**•, R = ^{p}Tol, ^{R}Cp = Cp′	**1d**•, R = ^{p}An, ^{R}Cp = Cp′	**1e**•, R = Mes, ^{R}Cp = Cp′	**1f**•, R = C$_6$F$_5$, ^{R}Cp = Cp′	**1j**•, R = Et, ^{R}Cp = Cp	**1k**•, R = ^{i}Pr, ^{R}Cp = Cp	**1l**•, R = ^{t}Bu, ^{R}Cp = Cp
M$^+$	285 (5)	313 (5)	329 (12)	341 (4)	389 (4)	237 (13)	251 (3)	265 (13)
M$^+$ – CO	257	285 (3)	301	313	361 (7)	209 (16)	223 (3)	237 (11)
M$^+$ – 2CO	229 (100)	257 (100)	273 (100)	285 (100)	333 (100)	181 (67)	195 (18)	209 (70)
^{R}CpMnS$^+$	152	166	166 (5)	166 (1)	166 (1)	152 (6)	152 (2)	152 (100)
^{R}CpMn$^+$	120 (44)	134 (7)	134 (32)	134 (4)	134 (17)	120 (86)	120 (100)	120 (20)
MnSR$^+$	164	178 (8)	194 (7)	206 (10)	254 (3)	116	130	144
MnS$^+$	87 (1)	87	87 (2)	87 (3)	87 (2)	87 (24)	87 (3)	87 (6)
SR$^+$	109	123 (10)	139 (4)	151 (10)	199 (1)	61	75	89
R$^+$	77 (1)	91 (30)	107	119 (18)	167 (5)	29	43 (2)	57 (3)
^{R}Cp$^+$	65 (6)	79 (7)	79 (15)	79 (5)	79 (14)	65 (23)	65 (1)	65
Mn$^+$	55 (15)	55 (2)	55 (5)	55 (1)	55 (2)	55 (100)	55 (46)	55 (1)

Table III. Analytical Data for the Compounds [^{R}Cp(CO)$_2$Mn]$_2$SR$^+$PF$_6^-$ ([2$^+$][PF$_6^-$])

compd	radical complex; amt, mg (mmol)	yield,[a] mg (%)	mp,[b] °C	formula	anal. % found (% calcd)
2a$^+$	**1a**•; 100 (0.35)	53 (25)		$C_{20}H_{15}F_6Mn_2O_4PS$	C, 39.91 (39.62) H, 2.76 (2.49)
2b$^+$	**1b**•; 890 (2.7)	720 (42)		$C_{20}H_{14}F_6Mn_2NO_6PS\cdot CH_2Cl_2$	C, 34.69 (35.26) H, 2.22 (2.19)
2c$^+$	**1c**•; 720 (2.3)	340 (23)	70	$C_{23}H_{21}F_6Mn_2O_4PS$	C, 42.74 (42.61) H, 3.37 (3.26)
2d$^+$	**1d**•; 820 (2.5)	330 (20)	>170	$C_{23}H_{21}F_6Mn_2O_5PS$	C, 42.37 (41.58) H, 3.36 (3.19)
2e$^+$	**1e**•; 690 (2.0)	420 (31)	160	$C_{25}H_{25}F_6Mn_2O_4PS$	C, 44.36 (44.39) H, 3.65 (3.73) S, 4.76 (4.74)
2f$^+$	**1f**•; 330 (0.85)	170 (28)	120	$C_{22}H_{14}F_{11}Mn_2O_4PS$	C, 36.42 (36.49) H, 2.14 (1.95) S, 4.72 (4.43)
2g$^+$	**1g**•; 420 (1.7)	320 (32)	148	$C_{18}H_{19}F_6Mn_2O_4PS$	C, 36.90 (36.88) H, 3.34 (3.27) S, 5.36 (5.47)
2h$^+$	**1h**•; 650 (2.5)	660 (45)	>200	$C_{19}H_{21}F_6Mn_2O_4PS$	C, 37.99 (38.02) H, 3.55 (3.53) S, 5.28 (5.34)
2i$^+$	**1i**•; 140 (0.5)	70 (22)	124	$C_{20}H_{23}F_6Mn_2O_4PS$	C, 40.16 (39.10) H, 4.48 (3.77)

[a] Yields based on radical complex **1**•, i.e. maximum possible yield as based on stoichiometry 50%. [b] Decomposition.

above; EtSH 420 mg (6.8 mmol), ^{t}BuSH 600 mg (6.7 mmol)) was added 2.5 g of Ph$_3$C$^+$PF$_6^-$ (6.4 mmol) and the mixture stirred at room temperature for 1 h. The resultant dark green crude mixture was adsorbed on silanized silica gel. Purification by column chromatography (silanized silica gel 60, 25 cm × 3 cm, –25 °C; *n*-pentane–CH$_2$Cl$_2$ 1:1) and crystallization from CH$_2$Cl$_2$–Et$_2$O (1:1) afforded 1780 mg (33%) of [**2g**$^+$][PF$_6^-$] and 950 mg (17%) of [**2i**$^+$][PF$_6^-$], respectively.

Table IV. Mass Spectra[a] of the Compounds $[^{R}Cp(CO)_2Mn]_2SR^+$ (2^+)

	MS, m/z (rel intens, %)						
fragment ion	**2c**$^+$, R = ^{p}Tol, ^{R}Cp = Cp′	**2d**$^+$, R = ^{p}An, ^{R}Cp = Cp′	**2e**$^+$, R = Mes, ^{R}Cp = Cp′	**2f**$^+$, R = C_6F_5, ^{R}Cp = Cp′	**2g**$^+$, R = Et, ^{R}Cp = Cp′	**2h**$^+$, R = ^{i}Pr, ^{R}Cp = Cp′	**2i**$^+$, R = ^{t}Bu, ^{R}Cp = Cp′
M^+	503 (2)	519 (1)	531 (48)	579 (2)	441 (2)	455 (1)	469 (<1)
$M^+ - 2CO$	447 (10)	463 (<1)	475 (4)	523 (<1)	385	399 (<1)	413
L_nMSR^+	313 (61)	329 (7)	341 (12)	389 (41)	251 (16)	265 (3)	279 (5)
$L_nMSR + H$	314 (40)	330 (5)	342 (68)	390 (100)	252 (45)	266 (7)	280 (3)
$L_nMSR^+ - 2CO$	257 (100)	273 (9)	285 (22)	333 (11)	195 (7)	209	223 (5)
$L_nMSH^+ - 2CO$	167 (56)	167 (3)	167 (100)	167 (4)	167 (100)	167 (100)	167 (100)
$L_nM^+ + CO$	218 (63)	218 (36)	218 (7)	218 (13)	218 (25)	218 (17)	218 (18)
$L_nMH^+ + CO$	219 (68)	219 (45)	219 (18)	219 (41)	219 (75)	219 (53)	219 (21)
$RSH + H^+$	125	141 (100)	153 (48)	201	63	77	91 (28)
RSH^+	124	140 (71)	152 (11)	200 (2)	62	76	90 (18)
RS^+	123	139 (27)	151 (3)	199 (4)	61	75	89 (83)

[a] $L_nM = Cp'Mn(CO)_2$; DCI-positive ions, reactant gas isobutane.

Mass spectroscopic data for some of the compounds $[2^+][PF_6^-]$ are given in Table IV.

X-ray Structural Determinations. Summaries of crystallographic results are presented in Tables IX and XV. All data sets were collected on a Siemens-Nicolet R3 diffractometer. Solution and refinement of the structures were performed on a VAX computer with the crystallographic program system SHELXTL (G. M. Sheldrick, Universität Göttingen, 1985). The structures were solved by direct methods and refined by the usual combination of Fourier synthesis and partially anisotropic full-matrix least-squares refinement. Rigid-group refinement for cyclopentadienyl entities was used in several cases. Hydrogen atoms were placed in idealized positions with fixed C-H bond lengths. Solvate molecules and PF_6^- counterions show crystallographically resolved rotational disorder in some cases. Selected geometric data for **1a**$^•$ and **1f**$^•$ are given in Tables VII and VIII and for $[\mathbf{2b}^+][PF_6^-]\cdot{}^1/_2CH_2Cl_2$, $[\mathbf{2h}^+][PF_6^-]$, and $[\mathbf{2i}^+][PF_6^-]$ in Tables XIII and XIV. Full tables of positional and thermal parameters, including those of counterions and solvate molecules, and of the structure factor amplitudes are available as supplementary material.

Abbreviations: Cp = η^5-C_5H_5; Cp′ = η^5-$C_5H_4CH_3$; Cp* = η^5-$C_5(CH_3)_5$; Et = C_2H_5; ^{i}Pr = isopropyl, C_3H_7; ^{t}Bu = *tert*-butyl, C_4H_9; Ph = phenyl, C_6H_5; ^{p}Tol = *p*-tolyl, $CH_3C_6H_4$; ^{p}An = *p*-anisyl, $CH_3OC_6H_4$; Mes = mesityl, 2,4,6-$(CH_3)_3(C_6H_2)$; LiTCNQ = lithium 7,7,8,8-tetracyanochinodimethane; s = singlet; d = doublet; t = triplet; q = quartet; sp = septet; m = multiplet; $\Delta E = E_p^{Ox} - E_p^{Red}$; E_p = anodic or cathodic peak potential.

Results and Discussion

1. Syntheses and Properties of the Compounds 1$^•$.

a. Syntheses. The standard synthesis for the preparation of **1**$^•$ consists of a two-step, one-pot process: first ^{R}Cp(CO)$_2$Mn(THF)[12] reacts with 1 equiv of RSH and then oxidation of the yellow-orange primary product, presumed to be ^{R}Cp(CO)$_2$Mn(HSR),[15] by air (eq 1).

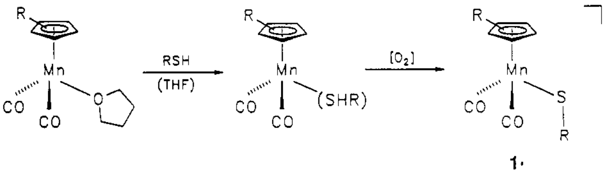

(1)

The oxidation process is an apparently instantaneous reaction accompanied by a color change from yellow-orange to the bright red or blue characteristic of the radical species **1**$^•$.

The numbering of the compounds **1**$^•$ chemically corresponds to the numbering of compounds **2**$^+$; e.g., **2a**$^+$ is obtained from **1a**$^•$ etc.

Table V. Infrared CO Stretching Frequencies for $[^RCp(CO)_2MnSR]^•$ (1$^•$) in CH_2Cl_2 at 298 K

	$[^RCp(CO)_2MnSR]^•$			
	^{R}Cp	R	color	ν(CO), cm^{-1}
1a$^•$	Cp	Ph	blue	1995 s, 1930 vs
1b$^•$	Cp	^{p}NO$_2$C$_6$H$_4$	red	1999 s, 1938 vs[a]
1c$^•$	Cp′	^{p}Tol	blue	1988 s, 1924 vs
1d$^•$	Cp′	^{p}An	blue	1986 s, 1922 vs
1e$^•$	Cp′	Mes	red	1990 vs, 1923 vs
1f$^•$	Cp′	C_6F_5	orange-red	2008 s, 1946 vs
1g$^•$	Cp′	Et	red	1986 vs, 1919 vs
1h$^•$	Cp′	^{i}Pr	red	1984 vs, 1917 vs
1i$^•$	Cp′	^{t}Bu	red	1980 vs, 1917 vs
1j$^•$	Cp	Et	red	1985 s, 1920 vs
1k$^•$	Cp	^{i}Pr	red	1982 vs, 1917 vs
1l$^•$	Cp	^{t}Bu	red	1989 s, 1925 vs
1m$^•$	Cp*	^{t}Bu	red	1974 s, 1908 s[b]

[a] In toluene. [b] In *n*-pentane.[2,3]

Analytically pure crystalline compounds **1**$^•$ are obtained in yields between 30 and 60% after chromatography and recrystallization.

Since reaction 1 afforded acceptable yields in all cases, not too much time was spent in searching for alternative routes to these compounds. It was, however, observed in the case of **1b**$^•$ that disulfides react with ^{R}Cp(CO)$_2$Mn(THF) directly to give **1**$^•$ (eq 2). This reaction is used for

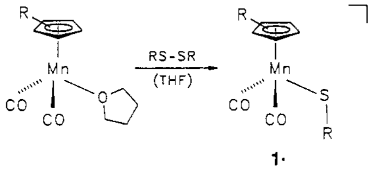

(2)

the preparation of selenium analogues of **1**$^•$, $[^RCp(CO)_2MnSeR]^•$.[3,10b]

b. Magnetic Data. From the series of compounds **1**$^•$ three were selected (**1a**$^•$, **1e**$^•$, **1f**$^•$) and used to establish the general magnetic behavior with use of all the techniques locally available. For the other compounds **1**$^•$ solution EPR spectra were taken, and only in the cases of **1b**$^•$ and **1g–i**$^•$, where the radicals were immediately transformed into the corresponding cations **2**$^+$, does the identity of **1**$^•$ rely upon IR data alone (Table V).

Results of the different types of magnetic measurements are shown in Table VI: solution EPR spectra reveal a sextet of lines with g_{iso} centered around 2.025 and coupling constants $a(^{55}Mn)$ between 5.0 and 5.5 mT. The EPR spectra in frozen solution indicate the approximate axial symmetry of the **g** tensor (Table VI). The coupling constant $a(^{55}Mn)$ could only be determined for g_1 and was found to be around 10 mT for this principal component of the tensor (Table VI). The kinds of spectra observed

---

[15] (a) Winter, A.; Scheidsteger, O.; Huttner, G. *Z. Naturforsch.* **1983**, *B38*, 1525. (b) Winter, A.; Zsolnai, L.; Huttner, G. *J. Organomet. Chem.* **1984**, *269*, C29.

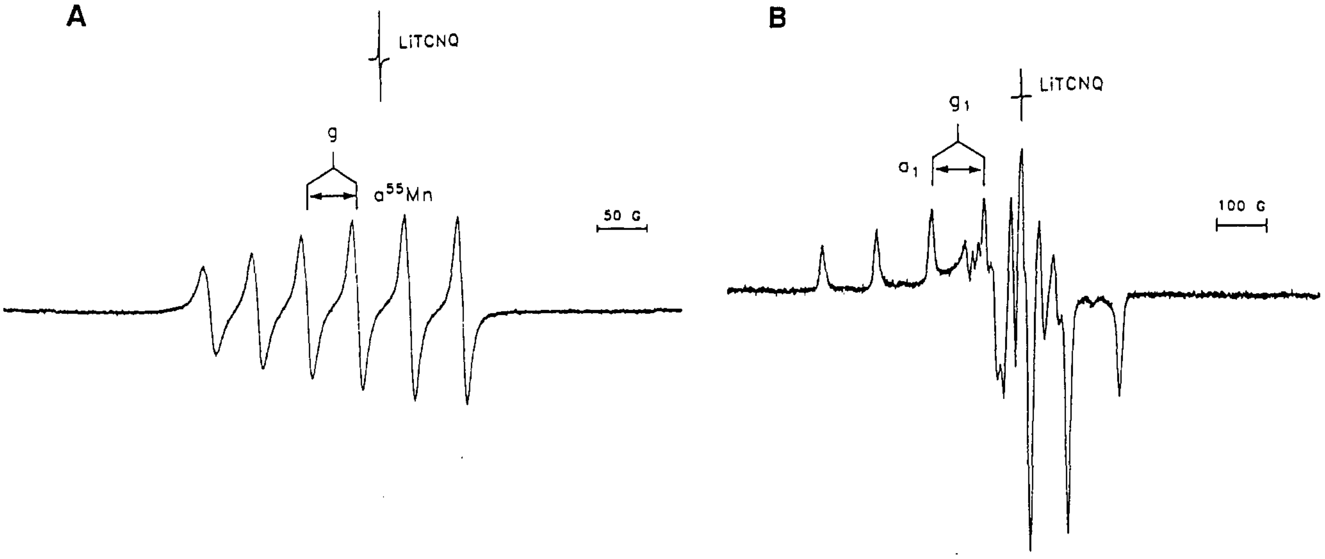

Figure 1. EPR spectra of [Cp′(CO)$_2$MnSC$_6$F$_5$]$^{\bullet}$ (**1f**$^{\bullet}$) in toluene at (A) 298 K and (B) 113 K (frequency 9.05 GHz).

Table VI. EPR Parameters and Magnetic Moments for [^{R}Cp(CO)$_2$MnSR]$^{\bullet}$ (1$^{\bullet}$)

compd	g_{iso} (a(^{55}Mn), mT)		μ_{eff} (solid state/soln), μ_B
1a$^{\bullet}$	2.0200 (5.5)^a	g_1 = 2.0575^c $g_{2,3}$ = 2.0114	1.71/1.60^d
1c$^{\bullet}$	2.0318 (5.0)^b	g_1 = 2.0681 (9.4) $g_{2,3}$ = 1.977	
1d$^{\bullet}$	2.0291 (5.1)^b	g_1 = 2.0682 (9.6) $g_{2,3}$ = 1.975	–/2.06^d
1e$^{\bullet}$	2.0315 (5.1)^b	g_1 = 2.0730 (10.5) $g_{2,3}$ = 1.959	1.67/1.74^d
1f$^{\bullet}$	2.0261 (5.6)^b	g_1 = 2.0804 (10.3) $g_{2,3}$ = 1.980	1.60/1.82^d
1j$^{\bullet}$	2.0270 (5.0)^a		
1k$^{\bullet}$	2.0272 (5.0)^a		
1l$^{\bullet}$	2.0215 (5.5)^a		
1m$^{\bullet}$	2.0306 (5.5)^a		1.62/–

^{a} In CH$_2$Cl$_2$. ^{b} In toluene. ^{c} Powder spectrum. ^{d} In acetone-d_6–1% TMS, at 298 K.

are shown in Figure 1 for the solution and the glass spectra of **1f**$^{\bullet}$.

Solid-state susceptibility measurements were performed on **1a**$^{\bullet}$, **1e**$^{\bullet}$, **1f**$^{\bullet}$, and **1m**$^{\bullet}$ in the temperature range between 130 and 298 K. The temperature dependence of χ follows the Curie–Weiss law. The corresponding magnetic moments are found to lie between 1.60 and 1.71 μB (Table VI), close to the expected spin-only value of 1.73 μB. Although the solid-state structures of **1a**$^{\bullet}$ and **1f**$^{\bullet}$ definitely contain monomeric entities (see below), there might in principle be some association in solution. NMR solution susceptibility measurements[16] at room temperature were therefore performed on **1a**$^{\bullet}$ and **1d–f**$^{\bullet}$. The susceptibility measured in solution closely corresponds to the magnetic moments found in the solid state and hence to the moment expected in a spin-only approximation (Table VI). In addition, the magnetic moments were found to be independent of the concentration of the sample. The magnetic data clearly establish the fact that complexes **1**$^{\bullet}$ are stable monomeric radical compounds. This evidence is especially useful with respect to the heavier analogues of **1**$^{\bullet}$ [^{R}Cp(CO)$_2$MnER]$_n$ (E = Se, n = 1, 2; E = Te, n = 2), which are either dimeric in all hitherto examined cases for E =

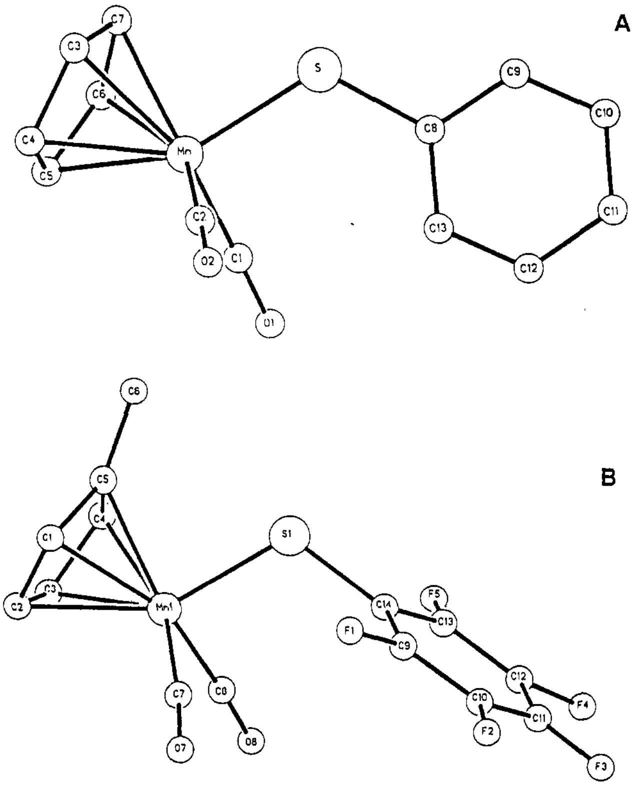

Figure 2. Molecular structure of (A) [Cp(CO)$_2$MnSPh]$^{\bullet}$ (**1a**$^{\bullet}$) and (B) [Cp′(CO)$_2$MnSC$_6$F$_5$]$^{\bullet}$ (**1f**$^{\bullet}$).

Table VII. Selected Bond Distances (Å) and Bond Angles (deg) for [Cp(CO)$_2$MnSPh]$^{\bullet}$ (1a$^{\bullet}$)

	Distances		
Mn–S	2.177 (2)	C1–O1	1.141 (4)
Mn–C1	1.790 (3)	C2–O2	1.138 (5)
Mn–C2	1.790 (3)	S–C8	1.759 (4)
Mn–C$_{Cp}$^{a}	2.145	C–C$_{Ar}$^{a}	1.378
	Angles		
Mn–S–C8	118.6 (1)	C1–Mn–C2	88.8 (1)
S–C8–C9	118.6 (1)	S–C8–C13	125.4 (3)
	Torsion Angles		
Mn–S–C8–C9	173.8		
Cx–Mn–S–C8	–177.1^b		

^{a} Average. ^{b} Cx = centroid of the ^{R}Cp ring.

---

[16] (a) Evans, D. F. *J. Chem. Soc.* **1959**, 2003. (b) Deutsch, J. L.; Poling, S. M. *J. Chem. Educ.* **1969**, *46*, 167. (c) Crawford, T. H.; Swanson, J. *J. Chem. Educ.* **1971**, *48*, 382.

Table VIII. Selected Bond Distances (Å) and Bond Angles (deg) for [Cp′(CO)$_2$MnSC$_6$F$_5$]$^\bullet$ (1f$^\bullet$)

	Distances		
Mn–S	2.205 (3)	S–C14	1.768 (7)
Mn–C7	1.818 (8)	C–C$_{Ar}$^{a}	1.395 (1)
Mn–C8	1.804 (8)	C9–F1	1.303 (8)
Mn–C$_{Cp}$^{a}	2.164	C10–F2	1.315 (9)
C7–O7	1.15 (1)	C11–F3	1.341 (9)
C8–O8	1.15 (1)	C12–F4	1.315 (8)
C–C$_{Cp'}$^{a}	1.420 (1)	C13–F5	1.298 (8)
C5–C6	1.47 (1)		
	Angles		
Mn–S–C14	111.6 (2)	S–C14–C9	120.1 (2)
C7–Mn–C8	88.2 (4)	S–C14–C13	119.8 (2)
	Torsion Angles		
Mn–S–C14–C13	−86.7		
Mn–S–C14–C9	96.9		
Cx–Mn–S–C14	−179.8^b		

^{a} Average. ^{b} Cx = centroid of the ^{R}Cp ring.

Table IX. Summary of X-ray Diffraction Data for [Cp(CO)$_2$MnSPh]$^\bullet$ (1a$^\bullet$) and [Cp′(CO)$_2$MnSC$_6$F$_5$]$^\bullet$ (1f$^\bullet$)

param	1a$^\bullet$	1f$^\bullet$
formula	$C_{13}H_{10}MnO_2S$	$C_{14}H_7F_5MnO_2S$
mw	285.22	389.20
space group (No.)	$P\bar{1}$ (2)	$C2/c$ (15)
a, Å	7.343 (5)	18.140 (5)
b, Å	7.435 (4)	12.408 (5)
c, Å	11.640 (6)	14.355 (5)
α, deg	101.83 (4)	90
β, deg	94.18 (5)	116.92 (2)
γ, deg	101.30 (4)	90
cell vol, Å^3	605.7 (5)	2881 (2)
Z	2	8
cryst dimens, mm	0.2 × 0.2 × 0.3	0.3 × 0.3 × 0.2
ρ(calc), g/cm^3	1.564	1.346
μ, cm^{-1}	0.125	0.084
temp, °C	−40	+20
radiatn, Å^c	Mo Kα	Mo Kα
2θ limits, deg	$2.0 < 2\theta < 43.0$	$2.0 < 2\theta < 54.0$
scan speed, deg/min	$2.0 < \dot{\omega} < 29.3$	$2.8 < \dot{\omega} < 24.3$
no. of rflns	1688 (1548)	3149 (2306)
no. of params refined^d	109	188
R^a	0.0355	0.0854
R_w^{b}	0.0359	0.0798

^{a} $\sum|F_o - F_c|/\sum|F_c|$. ^{b} $[\sum w(|F_o - F_c|)^2/\sum wF_o^2]^{1/2}$. ^{c} λ(Mo Kα) = 0.71073 Å. ^{d} Number of reflections measured (number of reflections with $I > 2\sigma$).

Table X. UV/Visible Spectroscopic Data for the Compounds 1$^\bullet$ in CH$_2$Cl$_2$ at 298 K

compd	λ, nm (ϵ, L mol^{-1} cm^{-1})			
1a$^\bullet$	580 (2850)	500 sh (2200)	390 (1500)	
1c$^\bullet$	600 (3000)	490 (1940)	390 sh (1680)	
1d$^\bullet$	630 (3240)	480 (1900)	400 sh (1550)	340 (6750)
1e$^\bullet$		510 (2310)		320 (6290)
1f$^\bullet$		460 (3410)		340 (2960)
1m$^\bullet$		510 (1250)		320 (2950)

Te[17] or in the case of E = Se exist as monomers or as dimers in the solid state, depending on R.[3,18]

c. Solid-State Structures. The results obtained by X-ray analyses for **1a**$^\bullet$ and **1f**$^\bullet$ are shown in Figure 2 and Tables VII–IX. The crystals of **1a**$^\bullet$ and **1f**$^\bullet$ are built from monomeric entities. The closest S–S distances within the crystal are 4.55 Å for **1a**$^\bullet$ and 5.52 Å for **1f**$^\bullet$ and are thus far beyond the range indicative of any direct interaction.

In both compounds the idealized mirror plane of the ^{R}Cp(CO)$_2$Mn fragment almost coincides with the plane containing the sulfur center and its two nearest neighbors (Mn, S, C14; **1f**$^\bullet$; Mn, S, C8, **1a**$^\bullet$; Figure 2, Tables VII and VIII). The observed orientation allows for the maximum overlap between the sulfur p orbital and the "better" one of the two d-type donor orbitals at the manganese center.[19] This type of orientation is also found for **1m**$^\bullet$.[2]

The most striking difference between the structures of **1a**$^\bullet$ and **1f**$^\bullet$ is the relative orientation of the aryl ring planes: the phenyl substituent of **1a**$^\bullet$ is almost coplanar with the coordination plane of the sulfur center, whereas the orientation relative to this plane is almost vertical for the C$_6$F$_5$ residue in **1f**$^\bullet$ (Figure 2, Tables VII and VIII).

While one may argue that this difference might have an electronic origin with the orientation found for **1a**$^\bullet$ maximizing and that found for **1f**$^\bullet$ minimizing arene–sulfur π-overlap, it is felt that the observed difference is as well explained by intra- and intermolecular forces within the crystal (for instance, a 90° rotation of the C$_6$F$_5$ residue in **1f**$^\bullet$ would already be expected to cause internal steric strain).

The fact that compounds [^{R}Cp(CO)$_2$MnSR]$^\bullet$ (**1**$^\bullet$) are available for nonconjugating alkyl substituents R (cf. Table V) gives further credibility to this kind of basically steric argument.

d. Infrared and UV/Visible Spectra. The compounds **1**$^\bullet$ without exception show two ν(CO) IR bands (Table V) which are expected for the geometry as shown in Figure 2. The general trend in absorption energies follows the relative tendency of the sulfur-bound residues to donate or withdraw electrons. The longest wavelength absorptions are found for R = alkyl as the inductively most donating substituents (Table V). For the derivatives **1a–f**$^\bullet$ a variation induced by the aryl substituents is evident with the strongest effect observed for the C$_6$F$_5$ substituent in **1f**$^\bullet$, which shows the shortest wavelength absorptions in the series **1**$^\bullet$ (Table V).

Since all compounds **1**$^\bullet$ show intense colors (Table V), the UV/vis spectra were recorded for a selection of compounds **1**$^\bullet$; these same compounds were also analyzed by cyclic voltammetry (see Table X). The data obtained allow for a more detailed discussion in the case of the aryl substituted derivatives **1a**$^\bullet$ and **1c–f**$^\bullet$.

The absorptions below 400 nm are pertinent to any ^{R}Cp(CO)$_2$MnL compound and are thus not especially connected to the radical chromophoric center. The strong absorptions above those wavelenths are characteristic for the radical compounds **1**$^\bullet$. At first sight the data appear somewhat confusing because either one (**1e**$^\bullet$, **1f**$^\bullet$) or two (**1a**$^\bullet$, **1c**$^\bullet$, **1d**$^\bullet$) bands are observed in this region. The characteristic phenotypes of the two sorts of spectra are shown in Figure 3.

Initial considerations were based on the assumption that monomer ⇌ dimer equilibria exist for those compounds where two bands were observed.[20] Such equilibria, however, are ruled out by the solution susceptibility measurements (discussed previously) as well as by the observation that the UV/vis spectrum of **1d**$^\bullet$ displays the same two maxima in a temperature range between 193 and 298 K; the only change observed is a minor narrowing of the

---

(17) Braunwarth, H.; Schuler, S.; Huttner, G. Unpublished results.

(18) (a) Braunwarth, H.; Lau, P.; Schiemenz, B.; Huttner, G.; Zsolnai, L. To be submitted for publication. (b) Braunwarth, H. Dissertation, Universität Heidelberg, 1988.

(19) (a) Schilling, B. E. R.; Hoffmann, R.; Lichtenberger, D. L. *J. Am. Chem. Soc.* **1979**, *101*, 585. (b) See: Kostic, N. M. Fenske, R. F. *J. Organomet. Chem.* **1982**, *233*, 337. (c) Hofman, P. *Angew. Chem.* **1977**, *89*, 551.

(20) See: (a) Treichel, P. M.; Rosenhein, L. D. *Inorg. Chem.* **1984**, *23*, 4018. (b) Treichel, P. M.; Rosenhein, L. D.; Schmidt, M. S. *Inorg. Chem.* **1983**, *22*, 3960. (c) Treichel, P. M.; Rosenhein, L. D. *J. Am. Chem. Soc.* **1981**, *103*, 691.

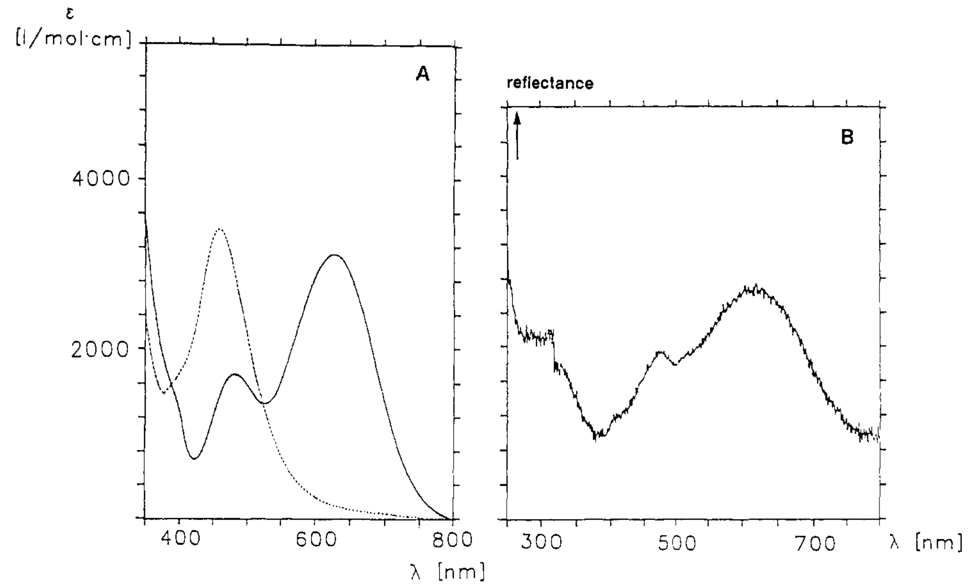

Figure 3. UV/vis spectra: (A) [Cp′(CO)$_2$MnS^{p}An]$^{\bullet}$ (**1d**$^{\bullet}$, ---) and [Cp′(CO)$_2$MnSC$_6$F$_5$]$^{\bullet}$ (**1f**$^{\bullet}$, —) in CH$_2$Cl$_2$; (B) crystalline **1d**$^{\bullet}$.

bands at lower temperature. Finally, the fact that the same type of spectrum is observed for crystalline **1d**$^{\bullet}$ (Figure 3B) definitely rules out any interpretation based on monomer ⇌ dimer equilibria.

The fact that **1e**$^{\bullet}$ (R = Mes) and **1f**$^{\bullet}$ (R = C$_6$F$_5$) have the same type of spectrum with only one relatively short wavelength absorption above 400 nm (Table X) contradicts any attempt to explain the observed differences on the basis of the varying donor–acceptor capabilities of the substituents R. The most probable explanation then is based on a correlation between the observed spectral phenotype and structure. As evidenced by X-ray analysis of **1a**$^{\bullet}$ and **1f**$^{\bullet}$, the planes of the aryl substituents may occupy different torsional positions. If it is assumed that bulky substituents at the ortho positions of the aryl substituent do not allow for the torsional position as observed for **1a**$^{\bullet}$ but force the aryl entity out of conjugation with the manganese–sulfur π system into the position observed for **1f**$^{\bullet}$, then the difference in the spectra of **1a**$^{\bullet}$, **1c**$^{\bullet}$, and **1d**$^{\bullet}$ on the one hand and **1e**$^{\bullet}$ and **1f**$^{\bullet}$ on the other is due to the presence (**1a**$^{\bullet}$, **1c**$^{\bullet}$, **1d**$^{\bullet}$) or absence (**1e**$^{\bullet}$, **1f**$^{\bullet}$) of conjugation between the manganese–sulfur π system and the aryl group. This interpretation is substantiated by the difference in redox behavior of **1a**$^{\bullet}$, **1c**$^{\bullet}$, and **1d**$^{\bullet}$ versus that of **1e**$^{\bullet}$ and **1f**$^{\bullet}$ upon cyclic voltammetric oxidation (see below).

e. Cyclic Voltammetry. The fact that compounds **1**$^{\bullet}$ are stable as monomeric radicals has been interpreted in terms of Mn$_{d_p}$–S$_{p_\pi}$ interactions,[2,3] which in the case of the electron-precise anions **1**$^-$ would comprise a two-center–four-electron repulsive π interaction (Figure 4).

Formation of the radicals **1**$^{\bullet}$ alleviates this repulsion, leaving only one electron in the antibonding π* orbital (Figure 4). This type of argument is intrinsically the same as that used to explain the relative stability of radicals such as SO$_2^{\bullet-}$, R$_3$N$_2^{\bullet}$, and R$_2$NO$^{\bullet}$;[21] in organometallic chemistry this argumentation has been put forward to explain the existence of stable paramagnetic aminyl complexes [Cp(CO)$_2$Mn(NHR)]$^{\bullet}$.[22] Compounds **1**$^{\bullet}$ are in a sense isoelectronic analogues of these aminyl species.

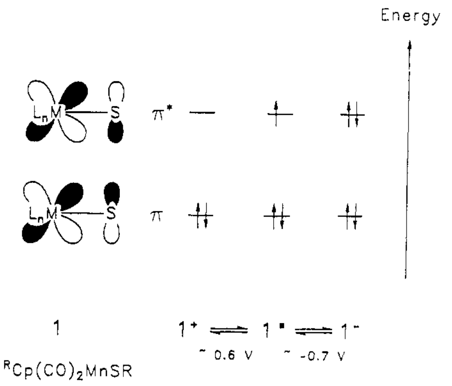

Figure 4. Occupation of the Mn–S π system in [^{R}Cp(CO)$_2$MnSR]$^{\bullet}$ (**1**$^{\bullet}$) and its one-electron-oxidation (**1**$^+$) and -reduction (**1**$^-$) products.

Table XI. Cyclic Voltammetric Data for the Compounds [^{R}Cp(CO)$_2$MnSR]$^{\bullet}$ (1$^{\bullet}$) in CH$_2$Cl$_2$ ($E_{1/2}$ in V, ΔE in mV)

compd	$E_{1/2}$ (ΔE) redn	oxidn	ferrocene
1a$^{\bullet}$	−0.63 (180)	+0.70 (170)	+0.42 (150)
1c$^{\bullet}$	−0.71 (210)	+0.58 (160)	+0.46 (150)
1d$^{\bullet}$	−0.73 (130)	+0.47 (130)	+0.44 (210)
1e$^{\bullet}$	−0.82 (210)	+0.77^b	+0.45 (160)
1f$^{\bullet}$	−0.57 (130)	+1.02^b	+0.44 (150)
1l$^{\bullet a}$	−0.75 (80)	+0.55 (60)	+0.40 (100)
1m$^{\bullet}$	−1.07 (130)	+0.38 (120)	+0.42 (180)

^{a} In CH$_3$CN. ^{b} Irreversible, peak potential.

The π* SOMO of **1**$^{\bullet}$ acts as a kind of electron reservoir: cyclic voltammetry shows that the radicals **1**$^{\bullet}$ generally undergo reversible one-electron reduction and oxidation, respectively.[3]

In all the compounds **1**$^{\bullet}$ studied so far, the one-electron reduction to **1**$^-$ is fully reversible (Table XI). The trend represented in the reduction potentials is evident: electron-donating substituents either on ^{R}Cp (compare [^{R}Cp(CO)$_2$MnS^{t}Bu]$^{\bullet}$ (^{R}Cp = Cp, **1e**$^{\bullet}$; ^{R}Cp = Cp*, **1m**$^{\bullet}$) or on the sulfur-bound residue R (compare **1c**–**e**$^{\bullet}$) tend to make reduction more difficult; the electron-withdrawing substituent R = C$_6$F$_5$ (**1f**$^{\bullet}$), on the other hand, makes the system easier to reduce. With the same arguments appropriately exchanged, a similar trend is seen for the reversible one-electron oxidation (**1a**$^{\bullet}$, **1c**$^{\bullet}$, **1d**$^{\bullet}$, **1l**$^{\bullet}$, **1m**$^{\bullet}$). As

---

(21) Nelsen, S. F.; Kice, J. L. In *Free Radicals*; Kochi, J. K., Ed.; Wiley: New York, **1973**; Vol. II, pp 527, 711.

(22) (a) Sellmann, D.; Müller, J.; Hofmann, P. *Angew. Chem.* **1982**, *94*, 708; *Angew. Chem., Int. Ed. Engl.* **1982**, *21*, 691. (b) Sellmann, D.; Müller, J. *J. Organomet. Chem.* **1985**, *281*, 249.

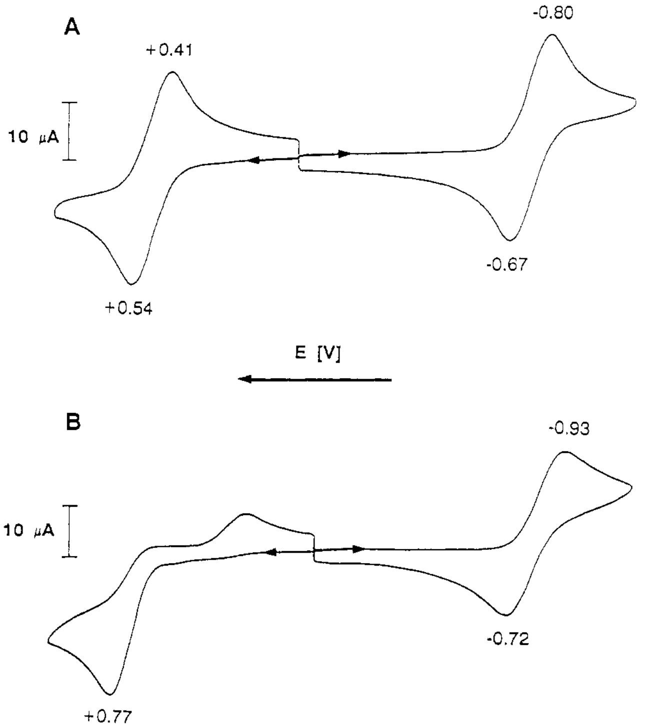

Figure 5. Cyclic voltammograms for the compounds [Cp'(CO)$_2$MnS^{p}An]$^•$ (**1d$^•$**, A) and [Cp'(CO)$_2$MnSMes]$^•$ (**1e$^•$**, B).

an exception, compounds **1e$^•$** and **1f$^•$** are only irreversibly oxidized. Even though this irreversibility does not allow for a strict comparison of the peak potentials of **1e$^•$** and **1f$^•$** with the values observed for the other members of the series **1$^•$**, the observed potentials are quite positive in relation to the rest of the oxidation potentials given in Table XI. For **1e$^•$** (R = Mes; Figure 5) the value of $E_p{}^a = +0.77$ V is quite counterintuitive with the electron-donating properties of the mesityl residue in mind. This exceptional behavior of **1e$^•$** and **1f$^•$** in the series of compounds **1$^•$** is exactly mirrored in their exceptional behavior regarding UV/vis spectroscopy (see section 1d)). It is assumed that the same reason is responsible for the peculiarities in the spectral as well as oxidation behavior of **1e$^•$** and **1f$^•$**: the large ortho substituents R = Mes, C$_6$F$_5$ impose a conformation on these species **1$^•$** which destabilizes the corresponding mononuclear cations **1e$^+$** and **1f$^+$**, respectively (cf. Figure 2).

2. Syntheses and Properties of the Compounds 2$^+$. a. Syntheses. If the oxidation of **1$^•$** is performed under the preparative conditions with the chemical oxidant AgPF$_6$, binuclear cations **2$^+$** are inevitably formed (eq 3).[5]

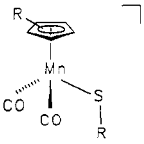

$$\xrightarrow[\text{toluene}]{\text{AgPF}_6} [^R\text{Cp(CO)}_2\text{Mn}]_2\text{SR}^+\ \text{PF}_6^- \qquad (3)$$

1$^•$ [2$^+$][PF$_6^-$]

Dependent on the nature of R, the cations **2$^+$** exist in one of the two isomeric forms A and B.

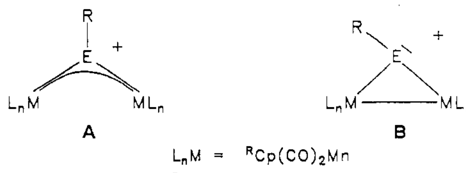

L$_n$M = ^{R}Cp(CO)$_2$Mn
^{R}Cp = Cp, Cp'
E = S, Se, Te

Table XII. Infrared CO Stretching Frequencies for [^{R}Cp(CO)$_2$Mn]$_2$SR$^+$ (2$^+$) in CH$_2$Cl$_2$ at 298 K

compd	^{R}Cp	R	color	ν(CO), cm^{-1}
2a$^+$	Cp	Ph	violet	2050 s, 2014 vs, 1985 s,[a] 1934 vw
2b$^+$	Cp	^{p}NO$_2$C$_6$H$_4$	violet	2055 s, 2021 vs, 1986 s,[a] 1935 vw
2c$^+$	Cp'	^{p}Tol	violet	2043 s, 2007 vs, 1975 m[a]
2d$^+$	Cp'	^{p}An	violet	2042 s, 2007 vs, 1974 m[a]
2e$^+$	Cp'	Mes	violet	2043 s, 2006 vs, 1976 m[a]
2f$^+$	Cp'	C$_6$F$_5$	violet	2053 m, 2022 vs, 1984 s,[a] 1941 vw
2g$^+$	Cp'	Et	green	2020 w, 1997 vs, 1971 s
2h$^+$	Cp'	^{i}Pr	green	2024 w, 1997 vs, 1969 s
2i$^+$	Cp'	^{t}Bu	green	2026 s, 1994 vs, 1967 m

[a] Broad.

The isomeric form B has been known for some time from the geometry of [Cp'(CO)$_2$Mn]$_2$SEt$^+$ (**2g$^+$**).[6] The alternative "inidene"-type structure A has been described for [Cp(CO)$_2$Mn]$_2$SPh$^+$ (**2a$^+$**).[5] The oxidation of **1$^•$** in toluene by AgPF$_6$ is a heterogeneous reaction. Upon addition of AgPF$_6$ the color of **1$^•$** gradually vanishes and a gray precipitate of [**2$^+$**][PF$_6^-$] and silver is formed. The PF$_6$ salt of **2$^+$** is extracted with CH$_2$Cl$_2$ and purified by crystallization.

An alternative synthesis of **2$^+$** avoids isolation of the precursor **1$^•$**. If the yellow-orange solutions obtained from ^{R}Cp(CO)$_2$Mn(THF) and RSH (see above) are not oxidized by air (where they give **1$^•$**) but instead by Ph$_3$CPF$_6$ (eq 4),

$$^R\text{Cp(CO)}_2\text{Mn(THF)} \xrightarrow[\text{THF}]{\text{RSH}} [^R\text{Cp(CO)}_2\text{Mn(SRH)}] \xrightarrow[\text{THF}]{\text{Ph}_3\text{CPF}_6} \underset{[2^+][\text{PF}_6^-]}{[^R\text{Cp(CO)}_2\text{Mn}]_2\text{SR}^+\ \text{PF}_6^-} \qquad (4)$$

compounds [**2$^+$**][PF$_6^-$] are immediately obtained. This procedure is only conceivably better than the one described in eq 3 because it demands the chromatographic purification of [**2$^+$**][PF$_6^-$].

b. Solid-State Structures of 2b$^+$, 2h$^+$, and 2i$^+$. Compounds **2$^+$** exist in two isomeric forms. The inidene-type geometry A has a trigonal-planar coordination at sulfur with a three-center-four-π-electron system delocalized over the Mn$\overset{\cdots}{-}$S(R)$\overset{\cdots}{-}$Mn part of the molecule. In the isomeric form B the four electrons delocalized in the π system of A are localized: two of them form a metal–metal bond, and the other two form a stereochemically active lone pair at the pyramidally coordinated sulfur of the RS bridging group.

For the compounds described here, X-ray analyses reveal the inidene-type arrangement A for **2b$^+$** (Figure 6, Tables XIII and XV) and the closed three-membered $\overline{\text{Mn–S–Mn}}$ cycle (arrangement B) for **2h$^+$** and **2i$^+$** (Figure 7, Tables XIV and XV).

2b$^+$ was crystallized as its PF$_6$ salt; the asymmetric unit of the triclinic unit cell contains two independent [**2b$^+$**][PF$_6^-$] entities and one CH$_2$Cl$_2$ solvate molecule. The geometric parameters of the two independent cations **2b$^+$** are almost identical (Table XIII). The coordination around sulfur is trigonal planar, the rms deviation from planarity amounting to only about 0.03 Å (0.035 Å for the cation shown in Figure 6 and 0.029 Å for the other independent cation **2b$^+$** in the crystal).

The angle subtended at the sulfur by the two manganese centers is around 136° (Table XIII) and is thus within the range typical for inidene-type compounds.[1,5] The Cp(CO)$_2$Mn entities are oriented in such a way that their idealized mirror planes are not very far from being coplanar with the coordination plane of the bridging sulfur (see Figure 6 and torsion angles in Table XIII). This type of arrangement maximizes the π interaction within the

Table XIII. Selected Bond Distances (Å) and Angles (deg) for [Cp(CO)$_2$Mn]$_2$S^{p}NO$_2$C$_6$H$_4$$^+$ (2b$^+$)^a

	Distances		
Mn1···Mn2	4.032/4.046	Mn1–C_{CO}^{b}	1.822/1.831
Mn1–S	2.178 (3)/2.178 (3)	Mn2–C_{CO}^{b}	1.826/1.829
Mn2–S	2.177 (3)/2.178 (3)	C–O^b	1.147/1.143
Mn1–C_{Cp}^{b}	2.159/2.157	S–C15	1.800 (6)/1.787 (7)
Mn2–C_{Cp}^{b}	2.153/2.145	C18–N	1.480 (9)/1.47 (1)
C–C_{Ar}^{b}	1.385/1.384	N–O^b	1.227/1.226
	Angles		
Mn1–S–Mn2	135.0 (1)/136.6 (1)		
Mn1–S–C15	113.2 (2)/112.0 (2)		
Mn2–S–C15	111.7 (2)/111.4 (2)		
C_{CO}–Mn1–C_{CO}	85.1 (3)/85.7 (3)		
C_{CO}–Mn2–C_{CO}	89.6 (3)/88.4 (3)		
O5–N–O6	124.1 (7)/122.4 (7)		
	Torsion Angles		
Cx(A)–Mn1–S–C15	14.6/6.7^c		
Cx(B)–Mn2–S–C15	18.1/13.3^c		
Cx(A)–Mn1–Mn2–Cx(B)	51.8/30.9^c		
Mn1–S–C15–C16	−90.1/−96.7		
Mn2–S–C15–C16	86.0/80.1		
Mn1–S–C15–C20	90.7/82.3		
Mn2–S–C15–C20	−93.1/−101.0		

^{a} Data for the two independent molecules **2b$^+$** in the crystal of [**2b$^+$**][PF$_6^-$]·$^1/_2$CH$_2$Cl$_2$ are given on one line separated by a slant. ^{b} Average. ^{c} Centroid of the Cp ring.

Table XIV. Selected Bond Distances (Å) and Angles (deg) for the Cations [Cp′(CO)$_2$Mn]$_2$S^{i}Pr$^+$ (2h$^+$) and [Cp′(CO)$_2$Mn]$_2$S^{t}Bu$^+$ (2i$^+$)

	2h$^+$	**2i$^+$**
	Bond Distances	
Mn1–Mn2	2.906 (1)	2.962 (1)
Mn1–S	2.253 (3)	2.267 (1)
Mn2–S	2.242 (2)	2.261 (1)
Mn1–C_{Cp}^{a}	2.167	2.165
Mn2–C_{Cp}^{a}	2.160	2.164
Mn1–C_{CO}^{a}	1.803	1.807
Mn2–C_{CO}^{a}	1.774	1.804
S–C_R	1.849 (7)	1.887 (4)^c
C–O^a	1.147	1.146
	Angles	
Mn1–S–Mn2	80.5 (1)	81.7 (1)
S–Mn1–Mn2	49.6 (1)	49.1 (1)
S–Mn2–Mn1	49.9 (1)	49.2 (1)
Mn1–S–C_R	113.8 (3)	117.7 (1)^c
Mn2–S–C_R	117.0 (2)	118.5 (1)^c
C_{CO}–Mn1–C_{CO}	84.9 (4)	83.8 (2)
C_{CO}–Mn2–C_{CO}	85.6 (4)	83.7 (2)
	Torsion Angles	
Cx–Mn1–Mn2–Cx	−153.5	32.8^b

^{a} Average. ^{b} Centroid of the Cp′ ring. ^{c} **2h$^+$**, C_R = C17; **2i$^+$**, C_R = C1.

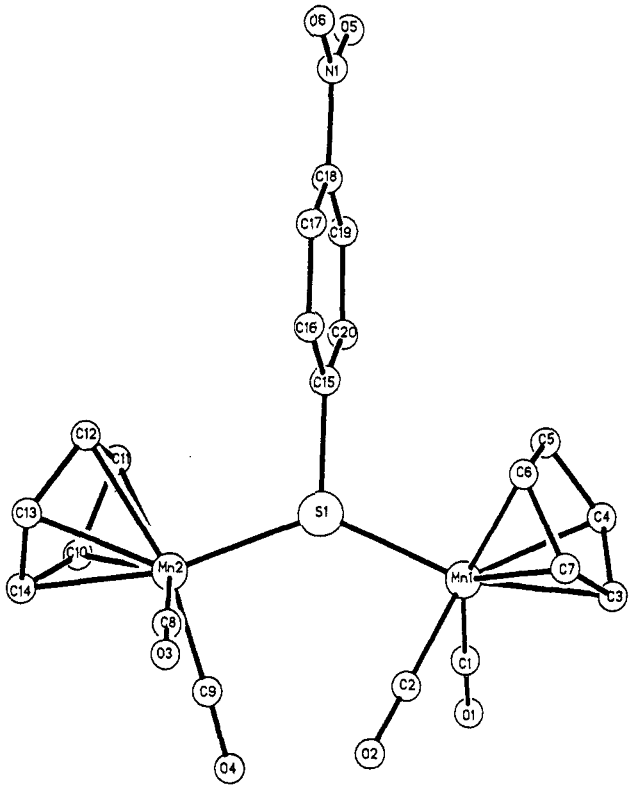

Figure 6. Molecular structure of [Cp(CO)$_2$Mn]$_2$S^{p}NO$_2$C$_6$H$_4$$^+$, the cation of [**2b$^+$**][PF$_6^-$].

three-center–four-π-electron system $\text{Mn}\overset{\frown}{-}\text{S(R)}\overset{\frown}{-}\text{Mn}$ and is characteristic for inidene compounds with Cp(CO)$_2$Mn termini.[19] In contrast, the aryl plane is in an orientation which minimizes the π interaction between the arene and the $\text{Mn}\overset{\frown}{-}\text{S(R)}\overset{\frown}{-}\text{Mn}$ π system. The corresponding torsion angles Mn–S–C$_\alpha$–C$_\beta$ are close to 90° (Table XIII). This again is the arrangement typically found in aryl-substituted inidene compounds.[1,5,23]

The isomeric structure B has been found for the cations **2h$^+$** and **2i$^+$** as their PF$_6$ salts (Figure 7, Tables XIV and XV). Both compounds contain closed $\overline{\text{Mn–S(R)–Mn}}$ cycles. The Mn–Mn distances are within the bonding range accepted for these elements[24] and similar to that reported for **2g$^+$** (2.930 Å for [**2g$^+$**][ClO$_4^-$][6]). The coordination around sulfur is pyramidal in both compounds **2h$^+$** and **2i$^+$** (Table XIV). The two cations differ in the torsional arrangement of the Cp′(CO)$_2$Mn entities. In **2h$^+$** the Cp′ ligands are approximately "trans" to each other (Figure 7, Table XIV). This type of arrangement appears to be common for RE$^+$-bridged [^{R}Cp(CO)$_2$Mn]$_2$ species;[6,25] in effect, it corresponds nicely to the idea that type B species might be formed in a conrotatory process from inidene-type compounds with a syn arrangement of the ^{R}Cp ligands as found for **2b$^+$** (Figure 6). The arrangement found for **2i$^+$** deviates from this common pattern, and the Cp′(CO)$_2$Mn group around Mn2 is in an orientation relative to the three-membered cycle which differs from "normal" (Figure 7). It is assumed that this kind of torsional arrangement is imposed onto **2i$^+$** by the bulky *tert*-butyl substituent.

c. ^{1}H NMR, Infrared, and UV/Visible Spectra. ^{1}H NMR spectra of **2i$^+$** when taken at 213 K show three different signals for the methyl substituents of the Cp′ rings. At room temperature one sharp signal is observed for each type of methyl group (Cp′, ^{t}Bu) in **2i$^+$** (Table XVI). Coalescence is observed at around 258 K. The dynamic behavior thus indicated is common to all species of type B independent of whether they contain RS$^+$ or RSe$^+$.[10] The observation of three different Cp′ signals in the low-temperature spectrum of **2i$^+$** shows that **2i$^+$** exists in more than just one isomeric form. In contrast, the low-temperature NMR spectra of **2g$^+$** and **2h$^+$** (213 K) give two sharp signals of equal intensity for the Cp-bonded

---

(23) The same type of structure is also found for the inidene-type compound [Cp′(CO)$_2$Mn]$_2$TeMes$^+$PF$_6^-$: Lau, P.; Huttner, G.; Zsolnai, L. To be submitted for publication.

(24) Mn–Mn bond lengths are shorter than 3.2 Å: (a) Herrmann, W. A.; Koumbouris, B.; Zahn, T.; Ziegler, M. L. *Angew. Chem.* **1984**, *96*, 802; *Angew. Chem., Int. Ed. Engl.* **1984**, *23*, 812. (b) Bernal, I.; Creswick, M.; Herrmann, W. A. *Z. Naturforsch.* **1979**, *B34*, 1345.

(25) Huttner, G.; Schuler, S.; Zsolnai, L.; Gottlieb, M.; Braunwarth, H.; Minelli, M. *J. Organomet. Chem.* **1986**, *299*, C4.

Table XV. Summary of X-ray Diffraction Data for $[Cp'(CO)_2Mn]_2S^iPr^+PF_6^-$ ($[2h^+][PF_6^-]$), $[Cp'(CO)_2Mn]_2S^tBu^+PF_6^-$ ($[2i^+][PF_6^-]$), and the CH_2Cl_2 Solvate of $[Cp(CO)_2Mn]_2S^pNO_2C_6H_4^+PF_6^-$ ($[2b^+][PF_6^-]\bullet{}^1/_2CH_2Cl_2$)

param	$[2h^+][PF_6^-]$	$[2i^+][PF_6^-]$	$[2b^+][PF_6^-]\cdot{}^1/_2CH_2Cl_2$
formula	$C_{19}H_{21}F_6Mn_2O_4PS$	$C_{20}H_{23}F_6Mn_2O_4PS$	$C_{20}H_{14}F_6Mn_2NO_6PS\cdot{}^1/_2CH_2Cl_2$
mw	600.28	614.30	693.70
space group (No.)	$P2_1/c$ (14)	$P\bar{1}$ (2)	$P\bar{1}$ (2)
a, Å	7.918 (4)	7.416 (1)	9.56 (7)
b, Å	25.58 (1)	12.823 (2)	13.62 (9)
c, Å	14.372 (6)	13.033 (3)	20.80 (2)
α, deg	90	86.76 (2)	86.86 (6)
β, deg	125.33 (3)	77.89 (2)	78.31 (6)
γ, deg	90	83.01 (1)	87.59 (6)
cell vol, Å^3	2375 (2)	1202 (1)	2649
Z	4	2	4
cryst dimens, mm	0.4 × 0.3 × 0.4	0.2 × 0.2 × 0.3	0.1 × 0.1 × 0.2
ρ(calc), g/cm^3	1.679	1.697	1.509
μ, cm^{-1}	0.129	0.128	0.115
temp, °C	+20	+20	−23
radiatn, Å[c]	Mo Kα	Mo Kα	Mo Kα
2θ limits, deg	$2.5 < 2\theta < 52.0$	$2.0 < 2\theta < 48.0$	$2.0 < 2\theta < 43$
scan speed, deg/min	$2.0 < \dot{\omega} < 29.3$	$2.6 < \dot{\omega} < 29.3$	$2.0 < \dot{\omega} < 29.3$
no. of rflns[d]	5238 (2596)	3769 (3343)	6940 (5007)
no. of refin params	100	309	648
R[a]	0.055	0.041	0.0561
R_w[b]	0.050	0.040	0.0518

[a] $\sum|F_o - F_c|/\sum|F_c|$. [b] $[\sum w(|F_o - F_c|)^2/\sum wF_o^2]^{1/2}$. [c] λ(Mo Kα) 0.710 73 Å. [d] Number of reflections measured (number of reflections with $I > 2\sigma$).

methyl groups. The observed spectra in this case (**2g**$^+$, **2h**$^+$) correspond to the "trans" arrangement, as found in the solid-state structure of $[2i^+][PF_6^-]$ (Figure 7). The coalescence temperature for the dynamic process is lowest for **2i**$^+$ (Table XVI). This corresponds to the results of a thermodynamic analysis of ring-opening/ring-closing processes for the related compounds $[^RCp(CO)_2Mn]_2SeR^+$,[10] where it is found that the ring-opening process B → A (eq 5) is entropically driven.

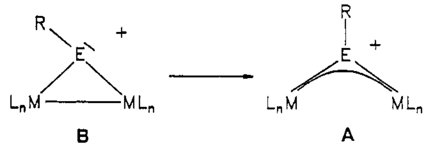

(5)

$L_nM = {}^RCp(CO)_2Mn$
^RCp = Cp, Cp'
E = S, Se, Te

Bulky substituents at the bridging main-group element make the formation of the open form A more favorable; in fact, $[^RCp(CO)_2Mn]_2SeR^+$ compounds which are stable in the inidene form A can only be obtained with bulky substituents such as R = Mes,[10,23] while with smaller substituents isomers of type B are formed.

On the basis of this knowledge it is to be expected that **2i**$^+$ with the bulky *tert*-butyl substituent will undergo a metal–metal bond-opening process more easily than the less bulky substituted species **2g**$^+$ and **2h**$^+$, respectively. The underlying assumption of this interpretation is that the dynamic behavior corresponds to a reversible metal–metal bond-opening process where the open form A allows for rotation of the $^RCp(CO)_2Mn$ fragments and is of course unbiased toward the inversion at sulfur and where the planar coordination around sulfur is halfway on the reaction coordinate of sulfur inversion.[26] These assumptions are experimentally verified in the case of the isoelectronic $[^RCp(CO)_2Mn]_2SeR^+$ compounds.[10]

The two isomeric forms of **2**$^+$ (A and B) are clearly differentiated by their UV/vis spectra. The inidene-type isomers A (**2a–f**$^+$) show the strong long-wavelength π–π^* absorption characteristic of their three-center–four-π-electron system (Figure 8) in the range between 550 and

Table XVI. ^{1}H NMR Data for the Compounds $[2^+][PF_6^-]$ in CD_2Cl_2 at 298 K

compd	^RCp/R	δ, ppm	T_C,[a] K
2a$^+$	Cp/Ph	5.29 (s, 10 H); 7.03 (m, 2 H); 7.45 (m, 3 H)	
2b$^+$	Cp/$^pNO_2C_6H_4$	5.37 (s, 10 H); 7.30 (m, 2 H); 8.31 (m, 2 H)	
2c$^+$	Cp'/^{p}Tol	1.93 (s, 6 H); 2.41 (s, 3 H); 5.09 (m, 4 H); 5.18 (m, 4 H); 6.91 (m, 2 H); 7.25 (m, 2 H)	*d*
2d$^+$	Cp'/^{p}An	1.91 (s, 6 H); 3.84 (s, 3 H); 5.06 (m, 4 H); 5.15 (m, 4 H); 6.93 (m, 4 H[b])	*d*
2e$^+$	Cp'/Mes	1.91 (s, 6 H); 2.04 (s, 6 H); 2.33 (s, 3 H); 4.94 (m, 4 H); 5.01 (m, 4 H); 6.97 (s, 2 H)	*d*
2f$^+$ [c]	Cp'/C_6F_5	1.92 (s, 6 H); 5.21 (m, 4 H); 5.37 (m, 4 H)	*d*
2g$^+$	Cp'/Et	1.77 (t, 3 H, J^{HH} = 7.2 Hz); 2.09 (s, 6 H); 3.34 (q, 2 H, J^{HH} = 7.2 Hz); 4.95 (m, 4 H); 5.16 (m, 4 H)	278
2h$^+$	Cp'/^{i}Pr	1.79 (d, 6 H, J^{HH} = 6.8 Hz); 2.10 (s, 6 H); 3.16 (sp, 1 H, J^{HH} = 6.8 Hz); 4.93 (m, 4 H); 5.16 (m, 4 H)	293
2i$^+$	Cp'/^{t}Bu	1.70 (s, 9 H); 2.11 (s, 6 H); 4.96 (m, 4 H); 5.18 (m, 4 H)	258

[a] Coalescence temperature for the signals of the Cp' ligand. [b] Broad. [c] ^{19}F NMR data (δ) for $[2f^+][PF_6^-]$: −76.8 (d, 6 F, J^{PF} = 711 Hz); −140.1 (d, 2 F, J^{FF} = 21 Hz); −151.9 (t, 1 F, J^{FF} = 16 Hz); 160.4 (m, 2 F). [d] No coalescence observed down to 210 K.

Table XVII. UV/Visible Spectroscopic Data for the Compounds $[2^+][PF_6^-]$ in CH_2Cl_2 at 298 K

compd	λ, nm (ϵ, L mol^{-1} cm^{-1})		
2a$^+$	560 (20 000)	440 (5 100)	340 (5 400)
2b$^+$	550 (16 400)	450 (4 300)	360 (7 100)
2c$^+$	600 (19 400)	480 sh (4 800)	340 sh (7 000)
2d$^+$	600 (11 300)	470 (3 200)	360 (5 200)
2e$^+$	570 (22 500)	450 (5 400)	330 (9 000)
2f$^+$	560 (22 800)	450 (12 600)	360 (13 200)
2g$^+$	570 (1 500)	420 (10 600)	330 (5 500)
2h$^+$		450 (10 600)	370 (5 700)
2i$^+$		430 (8 900)	340 (5 100)

---

(26) For a review see: Abel, E. W.; Bhargava, S. K.; Orrell, K. G. *Prog. Inorg. Chem.* **1984**, *32*, 1.

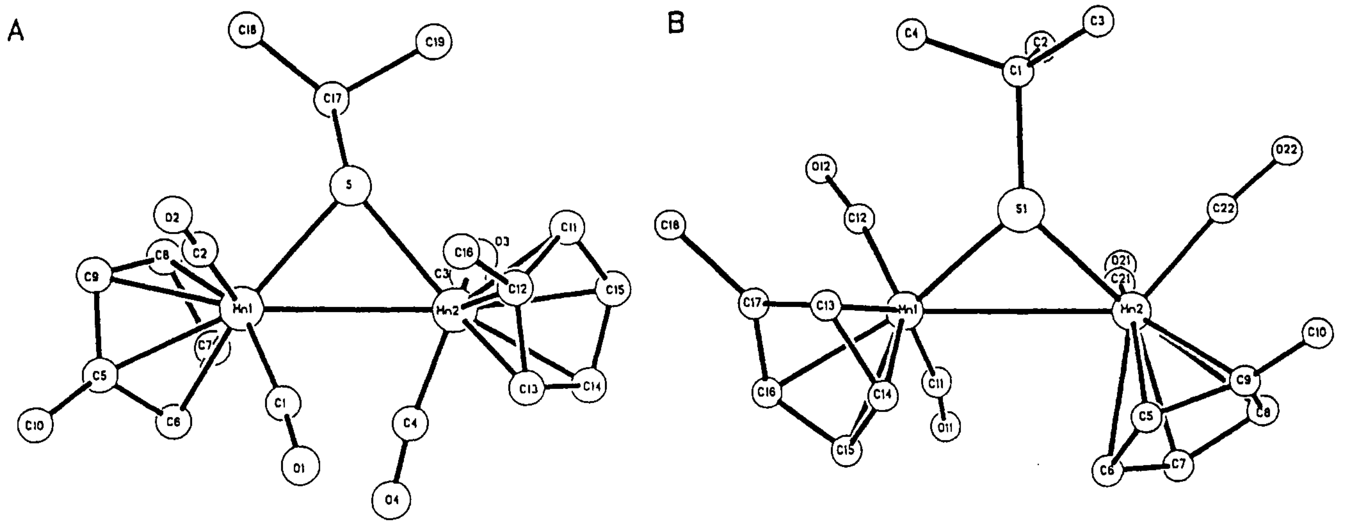

Figure 7. Molecular structures of the cations [$Cp'(CO)_2Mn]_2S^iPr^+$ ($\mathbf{2h^+}$, A) and [$Cp'(CO)_2Mn]_2S^tBu^+$ ($\mathbf{2i^+}$, B).

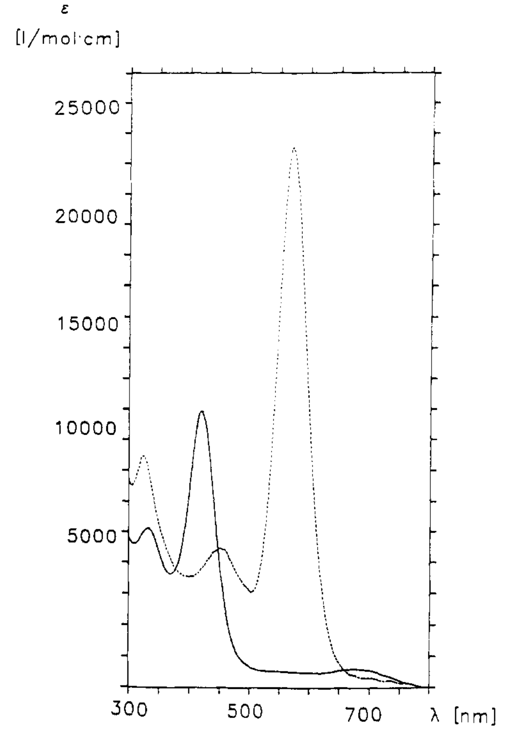

Figure 8. UV/vis spectra of the compounds [$Cp'(CO)_2Mn]_2S^iPr^+$ ($\mathbf{2h^+}$, - - -) and [$Cp'(CO)_2Mn]_2SMes^+$ ($\mathbf{2e^+}$, —) in CH_2Cl_2 at 298 K.

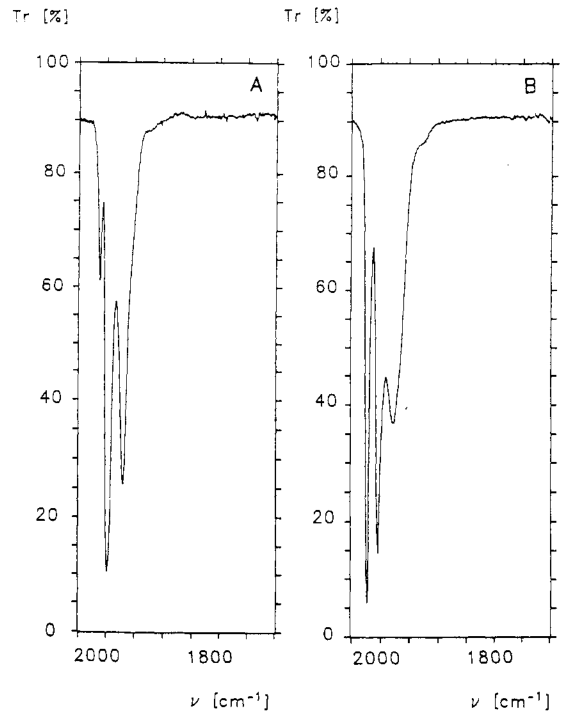

Figure 9. Infrared spectra in the CO stretching region of [$Cp'(CO)_2Mn]_2SMes^+$ ($\mathbf{2e^+}$, A) and [$Cp'(CO)_2Mn]_2S^iPr^+$ ($\mathbf{2h^+}$, B) in CH_2Cl_2 at 298 K (Tr = transmittance (%)).

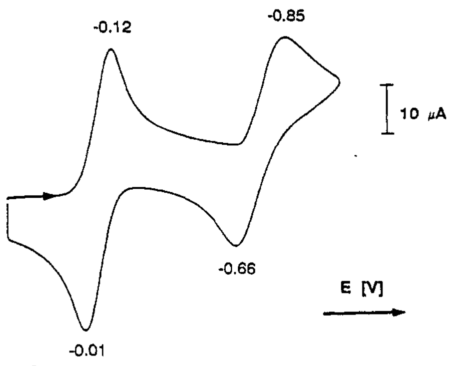

Figure 10. Cyclic voltammogram of [$Cp'(CO)_2Mn]_2SMes^+$ ($\mathbf{2e^+}$) in CH_2Cl_2 at 298 K.

600 nm ($\epsilon \approx 20000$ L/(mol cm); Table XVII). A second, less intense, higher energy absorption, while being characteristic of the inidene bonding system, is less discriminative because in the range where it is observed (440–480 nm) absorptions due to other $^RCp(CO)_2Mn$ chromophores may be present.

In the closed isomers B ($\mathbf{2g}$–$\mathbf{i^+}$) the prominent absorption in the spectral range between 800 and 300 nm is a band at around 420–450 nm ($\epsilon \approx 10000$ L(mol cm); Figure 8, Table XVII). This absorption is indicative of a metal–metal bond[27] and is quite characteristic for the isomers B. Since the absorptions typical of A and B are well separated in wavelength as well as in intensity, UV/vis spectroscopy is the analytical tool of choice for this type of chemistry. Figure 8 visualizes the two spectral phenotypes for the ring-closed isomers B and the inidene-type isomers A, taking $\mathbf{2h^+}$ and $\mathbf{2e^+}$ as characteritic examples.

IR spectra in the ν(CO) region are also helpful in differentiating the forms A and B of $\mathbf{2^+}$. The absorption

---

[27] Wrighton, M. S. *Top. Curr. Chem.* **1976**, *65*, 37.

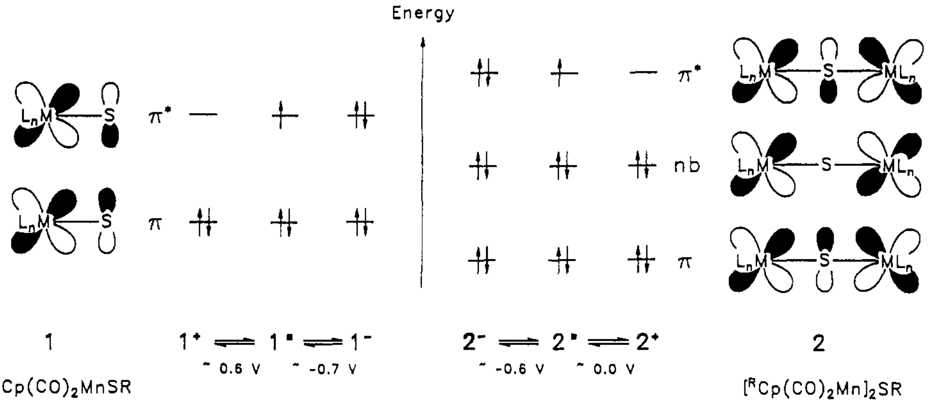

Figure 11. Comparison of the two-center olefinic type Mn⇁S π system in 1 and the three-center allylic type Mn⇁S⇁Mn π system in 2. The LUMO of 1^+ is necessarily lower in energy as compared to the LUMO of 2^+. The reduction potentials observed for 1^+ and 2^+ respectively substantiate this model.

Table XVIII. Cyclic Voltammetric Data for the Compounds [^{R}Cp(CO)$_2$Mn]$_2$SR$^+$ (2^+) in CH$_2$Cl$_2$ ($E_{1/2}$ in V, ΔE in mV)

	$E_{1/2}$ (ΔE)		
compd	1st redn	2nd redn	ferrocene
2a$^+$	−0.04 (110)	−0.56 (120)	+0.39 (140)
2b$^+$	+0.10 (80)	−0.35 (100)	+0.44 (130)
2c$^+$	−0.11 (140)	−0.63 (140)	+0.39 (130)
2d$^+$	−0.11 (80)	−0.61 (80)	+0.42 (140)
2e$^+$	−0.07 (110)	−0.75 (200)	+0.46 (150)
2f$^+$	+0.10 (100)	−0.50 (110)	+0.39 (120)
2g$^+$	−0.14 (130)	−0.63 (130)	+0.40 (120)
2h$^+$	−0.14 (140)	−0.66 (150)	+0.44 (130)

patterns of the two isomeric forms differ in the relative intensities of the three highest energy bands (Figure 9, Table XII) with the band having the third highest energy being broad for type A isomers and narrow for type B isomers. A stronger discriminator is the energy of the two highest energy bands, which is definitely higher for isomers A (**2a**–**f**$^+$) as compared to isomers B (**2g**–**i**$^+$; Table XII).

d. Cyclic Voltammetry of [2$^+$][PF$_6^-$]. Cyclic voltammetric data have been collected for **2a**–**h**$^+$ (Table XVIII). All the cations 2^+ show two reversible one-electron reductions. The reversibility of these electrode processes is not only inferred from the shape of the cyclic voltammetric curves (Figure 10) but also by an independent chemical check. The anion corresponding to **2e**$^+$, [Cp′(CO)$_2$Mn]$_2$SMes$^-$ (**2e**$^-$), has been serendipitously obtained as a byproduct of a reaction which was aimed at a completely different result.[11] Its structure has been determined by X-ray analysis of its [Na$^+$(12-crown-4)$_2$] salt.[11] The geometry of **2e**$^-$ in general terms corresponds to the structures observed for the isoelectronic anions [Cp(CO)$_2$Mn]$_2$TeR$^-$ [25] and [(CO)$_5$Cr]$_2$S^{t}Bu$^-$.[4]

The anion **2e**$^-$ shows two reversible oxidation waves in its cyclic voltammogram; the $E_{1/2}$ values (−0.09, −0.76 V) obtained for the oxidation of the anion are equal to $E_{1/2}$ values given in Table XVIII for the reduction of the cation **2e**$^+$ (Figure 10).

The reduction behavior of 2^+ thus corresponds to the oxidation behavior of [(CO)$_5$Cr]$_2$SR$^-$, where two reversible one-electron-oxidation waves at around −0.4 and +1.0 V are observed.[4]

The first reduction potential of the species 2^+ is observed between −0.14 and +0.10 V for the compounds **2a**–**h**$^+$ (Table XVIII). It is only marginally dependent on the type of substituent R in [^{R}Cp(CO)$_2$Mn]$_2$SR$^+$ (2^+). The tendency observed is as expected: electron-withdrawing substituents such as R = ^{p}NO$_2$C$_6$H$_4$ (**2b**$^+$) and R = C$_6$F$_5$ (**2f**$^+$) make reduction easier as compared to electron-donating substituents (Table XVIII). This trend is more pronounced for the second reduction: reduction is most difficult for **2e**$^+$ (R = Mes; $E_{1/2}$ = −0.75 V) and easiest for **2b**$^+$ (R = ^{p}NO$_2$C$_6$H$_4$; $E_{1/2}$ = −0.35 V). These two compounds mark the extremes in the range of values observed for the process $2^\bullet \rightleftharpoons 2^-$.

The related pairs of compounds $1^\bullet$ and 2^+ show distinctly different cyclic voltammograms (Tables XI and XVIII). In the cyclic voltammograms of 2^+ there is no indication of any fragmentation possibly leading to 1^+ nor is there any indication of the formation of 2^+ from 1^+ under the cyclic voltammetric conditions, even though 2^+ is obtained from $1^\bullet$ upon chemical oxidation with AgPF$_6$.

It is noteworthy that the series of compounds **2g**–**i**$^+$ existing as ring-closed isomers B show the same cyclic voltammetric behavior as the inidene-type isomer A (**2a**–**f**$^+$). It has already been mentioned (see section 2c) that species of type B are in equilibrium with their type A isomers. The similarity in the redox behavior of all compounds 2^+, irrespective of whether they are members of the A or B isomer family, may then be explained by the assumption that the species which are electrochemically active at the electrode surface under the conditions applied are alike for all compounds 2^+. With respect to the open structure of the reduced species and to the reversibility of the redox processes in all cases it is probable that the electroactive species is of the isomeric type A.

The complete series of cyclic voltammetric data for the related pairs of compounds [^{R}Cp(CO)$_2$MnSR]$^+$ (1^+) and [^{R}Cp(CO)$_2$Mn]$_2$SR$^+$ (2^+) allows for a conclusive comparison. In each case the LUMO of the cation (1^+, 2^+) is a π* antibonding orbital made up of manganese and sulfur π-type orbitals.[1-3,5,22] There are two interacting π centers in $1^\bullet$ and three in $2^\bullet$. The greater number of π interactions in $2^\bullet$ leads to a larger splitting between π and π*, as is well-known for the archetypal pair of model compounds ethylene and allyl.[28,29] Consistent with this analysis the cations 1^+ are easier to reduce than the cations 2^+, the difference amounting to some 0.6 V (Figure 11).

The simple one-electron model cannot be expected to indicate what energy is necessary to add a second electron into the singly occupied π* SOMO of $1^\bullet$ or $2^\bullet$. The data show that in both series of compounds this reduction needs about −0.6 to −0.7 V.

---

(28) Heilbronner, E.; Bock, H. In *Das HMO-Modell und seine Anwendung*; Weinheim, Germany, **1976**; Vol. III.

(29) An extended Hückel calculation on [Cp(CO)$_2$MnSH]$^+$ and [^{R}Cp(CO)$_2$Mn]$_2$SH$^+$ gives (quite independent of the individual Hückel parameters used) consistently a lower energy for the π* orbital of the mononuclear compounds as compared to the energy of the π* LUMO of the binuclear inidene-type species.

Organometallics 1991, *10*, 3873–3876

Acknowledgment. We thank Dr. Hans Grützmacher for the ^{19}F NMR spectra, Sabine Fiedler and Stephan Pitter for magnetic measurements and mass spectra, and also the staff of the microanalytical laboratory of the University of Heidelberg. We also thank the Deutsche Forschungsgemeinschaft (Grant No. SFB 247) and the Fonds der Chemischen Industrie for the financial support of this work.

Registry No. **1a**$^\bullet$, 114095-82-8; **1b**$^\bullet$, 136378-96-6; **1c**$^\bullet$, 136378-97-7; **1d**$^\bullet$, 136378-98-8; **1e**$^\bullet$, 136378-99-9; **1f**$^\bullet$, 136379-00-5; **1g**$^\bullet$, 136379-01-6; **1h**$^\bullet$, 136379-02-7; **1i**$^\bullet$, 136379-03-8; **1j**$^\bullet$, 136379-04-9; **1k**$^\bullet$, 136379-05-0; **1l**$^\bullet$, 93530-59-7; **1m**$^\bullet$, 100687-97-6; [**2a**$^+$][PF_6^-], 114095-84-0; [**2b**$^+$][PF_6^-], 136379-07-2; [**2b**$^+$][PF_6^-]$\cdot{}^1/_2CH_2Cl_2$, 136379-20-9; [**2c**$^+$][PF_6^-], 136379-09-4; [**2d**$^+$][PF_6^-], 136379-11-8; [**2e**$^+$][PF_6^-], 136379-13-0; [**2f**$^+$][PF_6^-], 136379-15-2; [**2g**$^+$][PF_6^-], 136458-36-1; [**2h**$^+$][PF_6^-], 136379-17-4; [**2i**$^+$][PF_6^-], 136379-19-6; PhSH, 108-98-5; [$^pNO_2C_6H_4S]_2$, 100-32-3; ^{p}TolSH, 106-45-6; ^{p}AnSH, 696-63-9; MesSH, 1541-10-2; C_6F_5SH, 771-62-0; EtSH, 75-08-1; ^{i}PrSH, 75-33-2; ^{t}BuSH, 75-66-1; (η^5-C_5H_5)$(CO)_2$Mn(THF), 12093-26-4; (η^5-C_5H_4Me)$(CO)_2$Mn(THF), 51922-84-0; (η^5-C_5Me_5)$(CO)_2$Mn(THF), 86155-78-4.

Supplementary Material Available: Tables of positional and thermal parameters as well as additional drawings of **1a**$^\bullet$, **1f**$^\bullet$, [**2b**$^+$][PF_6^-]$\cdot{}^1/_2CH_2Cl_2$, [**2i**$^+$][PF_6^-], and [**2h**$^+$][PF_6^-] (15 pages); listings of observed and calculated structure factors (101 pages). Ordering information is given on any current masthead page.

Anionic (Nitrophenyl)palladium(II) Carbonyls. Crystal Structure of *cis*-[$PPh_3(CH_2Ph)$][$Pd(C_6H_3Me\text{-}2,NO_2\text{-}6)Cl_2(CO)$]

José Vicente,* Aurelia Arcas, and M. Victoria Borrachero

Grupo de Química Organometálica, Departamento de Química Inorgánica, Facultad de Ciencias Químicas, Universidad de Murcia, E-30171 Espinardo, Murcia, Spain

Antonio Tiripicchio* and Marisa Tiripicchio Camellini

Istituto di Chimica Generale ed Inorganica, Università di Parma, Centro di Studio per la Strutturistica Diffrattometrica del CNR, Viale delle Scienze 78, I-43100 Parma, Italy

Received March 28, 1991

Complexes [$PPh_3(CH_2Ph)$][$Pd(R)Cl_2(CO)$] [R = C_6H_3Me-2,NO_2-6 (**1**), $C_6H_2(NO_2)_3$-2,4,6 (**2**)] can be isolated by carbonylation, at room temperature and atmospheric pressure, of [$PPh_3(CH_2Ph)]_2[Pd(R)Cl(\mu\text{-}Cl)]_2$. Complex **1** is the first example of an organocarbonylpalladium(II) complex characterized by an X-ray diffraction study. Crystals are triclinic, space group $P\bar{1}$, with $Z = 2$ in a unit cell of dimensions $a = 10.446$ (5) Å, $b = 12.538$ (7) Å, $c = 14.148$ (6) Å, $\alpha = 65.40$ (2)°, $\beta = 74.17$ (2)°, and $\gamma = 72.83$ (2)°. The structure has been solved by Patterson and Fourier methods and refined by full-matrix least squares on the basis of 1274 observed reflections to R and R_w values of 0.0319 and 0.0440. In the anionic complex the Pd atom is in a square-planar arrangement with two Cl atoms in cis positions and the carbonyl group and the 2-methyl-6-nitrophenyl ligand trans to them. The Pd–CO bond [Pd–C = 1.853 (10) Å] is discussed on the basis of the IR and X-ray data.

Introduction

Palladium compounds have been used as catalysts in carbonylation and decarbonylation reactions.[1] In these processes the organic compounds are assumed to be obtained on the basis of the unstability of some carbonyl intermediates (Scheme I). Under this assumption it is easy to justify the low number of organocarbonylpalladium(II) complexes reported.[2] This difficulty adds to the general tendency of palladium(II) compounds to be reduced to palladium(I) or -(0) complexes by carbon monoxide[2a] and also to the lability of the Pd–CO bond.[2,3] Owing to all these factors, structural studies on palladium(II) carbonyls are based on spectroscopic (mainly IR) data. Only very recently the first crystal structures of two such compounds, [$PdX_3(CO)]^-$ (X = Cl, Br), have been reported.[3d]

Scheme I

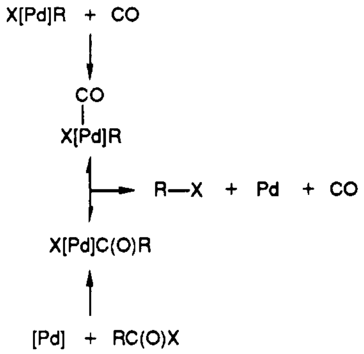

Calderazzo[3] and Uson[2b] have suggested a negligible π back-bonding contribution to the Pd(II)–CO bond on the basis of thermodynamic and spectroscopic data. Herein we report the preparation and IR data of two new carbo-

---

[1] Heck, R. F. *Palladium Reagents in Organic Syntheses*; Academic Press: New York, 1987; p 341.

[2] (a) Maitlis, P. M.; Espinet, P.; Russell, M. J. H. *Comprehensive Organometallic Chemistry*; Pergamon: London, 1982; Vol. 6, p 279. (b) Usón, R.; Forniés, J.; Tomás, M.; Menjón, B. *Organometallics* **1985**, *4*, 1912.

[3] (a) Calderazzo, F.; Belli Dell'Amico, D. *Inorg. Chem.* **1981**, *20*, 1310. (b) Belli Dell'Amico, D.; Calderazzo, F.; Zandonà, N. *Inorg. Chem.* **1984**, *23*, 137. (c) Belli Dell'Amico, D.; Calderazzo, F.; Veracini, C. A.; Zandonà, N. *Inorg. Chem.* **1984**, *23*, 3030. (d) Andreini, B. P.; Belli Dell'Amico, D.; Calderazzo, F.; Venturi, M. G.; Pelizzi, G. *J. Organomet. Chem.* **1988**, *354*, 389.

0276-7333/91/2310-3873$02.50/0